Journal of Materials Chemistry A

Accepted Manuscript

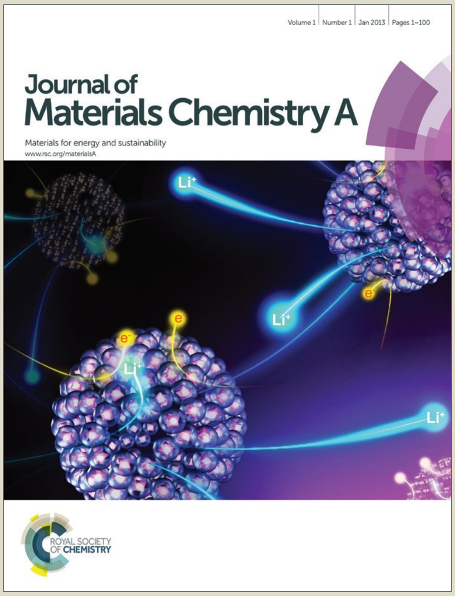
Volume 1 | Number 1 | Jan 2013 | Pages 1–100

Journal of Materials Chemistry A

Materials for energy and sustainability

www.rsc.org/materialsA

ROYAL SOCIETY OF CHEMISTRY

www.rsc.org/materialsA

Journal Name RSCPublishing

ARTICLE

Cite this: DOI: 10.1039/x0xx00000x

Received 00th January 2012,
Accepted 00th January 2012

DOI: 10.1039/x0xx00000x

www.rsc.org/

A Review of One-dimensional TiO_2 Nanostructured Materials for Environmental and Energy Applications

Mingzheng Ge,[a] Chunyan Cao,[a] Jianying Huang,[a,b] Shuhui Li,[a] Zhong Chen,[c] Ke-Qin Zhang,[a,b] S.S. Al-Deyab,[d] and Yuekun Lai*[a,b]

One-dimensional TiO_2 (1D TiO_2) nanomaterials with unique structural and functional properties have been extensively used in various fields including photocatalytic degradation of pollutants, photocatalytic CO_2 reduction into energy fuels, water splitting, solar cells, supercapacitors and lithium batteries. In the past a few decades, 1D TiO_2 nanostructured materials with well-controlled size and morphology has been designed and synthesized. Compared to 0D and 2D nanostructures, more attention has been paid to 1D TiO_2 nanostructures due to its high aspect ratio, large specific surface area, excellent electronic or ionic charge transport property. In this review, we present the crystal structure of TiO_2 and the latest development on the fabrication of 1D TiO_2 nanostructured materials. Besides, we will look into some critical engineering strategies that give rise to the excellent properties of 1D TiO_2 nanostructures such as improved enlargement of surface area, light absorption and efficient separation of electron/holes that benefit their potential applications. Moreover, their corresponding environmental and energy applications are described and discussed. With the fast development of the current economy and technology, more and more effort will be put into endowing TiO_2-based materials with advanced functionalities and other promising applications.

1. Introduction

The fast development of global economy and industrialization in the past century has also brought about serious problems to the world's population. Our rapacious consumption of fossil resources at the exponentially increasing rate has led to global warming and climate change. On the other hand, the extensive use of these energy sources has also caused much pollution on the environment.[1-3] This has aroused serious concerns over the need for renewable sources of clean energy and degradation of pollutants. For example, upon exposure to sunlight, solar energy can be utilized by photocatalysts to degrade organic pollutants, reduce CO_2 into renewable hydrocarbon solar fuels and produce hydrogen by water splitting.[4-6] Besides, supercapacitors, solar cells and lithium ion batteries are useful technology to overcome the shortage of nature resources.[7-9] These all strategies are promising to solve the environment contamination problems and energy crisis.

Titanium dioxide (TiO_2), since discovered for water photolysis by Fujishima and Honda in 1972,[10] has been paid much attention and widely used in photocatalytic degradation of pollutants,[11, 12] photocatalytic CO_2 reduction into energy fuels,[13,14] water splitting,[15, 16] solar cells,[17, 18] supercapacitors,[19, 20] biomedical devices[21, 22] and lithium ion batteries.[23, 24] Most initial investigations were focused on 0D TiO_2 nanoparticles and it showed excellent performances in photocatalysis, hydrogen production, solar cells, adsorbents and sensors due to large surface area and a broadened band gap.[25-28] However, it also showed unavoidable disadvantages such as fast recombination of electron and holes, slow charge carriers transfer and high recycling cost.[29, 30] The synthesis of 2D nanostructured materials was comparably complex and required harsh experimental conditions.[31-33] Recently, 1D nanostructure has been extensively studied due to its distinctive advantages. Generally, a 1D nanostructure had a high aspect ratio with the diameter ranging from 1 to 100 nm, and it can be in the tube-, rod-, wire-, fiber- or belt-shaped. Therefore, 1D TiO_2 nanostructured materials inherited all the typical features of TiO_2 nanoparticles and displayed a large specific surface area which is easy for photogenerated carriers to transfer along the axial direction. In addition, the relative easiness in its production adds into its advantages. Meanwhile, the relatively large specific surface area and chemical stability make it an ideal building block for assembling various surface heterostructures, allowing 1D TiO_2 nanostructured materials to be widely used in photocatalysis, water splitting and nanodevices.[34-37] However, the wide application of 1D TiO_2 nanostructured materials in some fields was limited due to several critical issues. Associated with the wide band gap, TiO_2 (anatase: 3.2 eV, rutile: 3.0 eV) occupies only 3-5% of the total solar spectrum. Besides, fast recombination of photogenerated electron-hole pairs also leads to decreased efficiency in the photocatalytic activity. What's more, a relatively low specific surface area on a smooth surface and a single crystal phase may pose certain constraints for it performaces.[38-41] Fortunately, 1D TiO_2 surface heterostructure can be designed and fabricated by introducing second phases with special morphology (nanoparticles, nanorods, nanowires)[42, 43] or doping with other materials (metals, non-metals, semiconductors)[44-46] to overcome the above-mentioned problems. As a result, light absorption can be broadened from the UV light to visible light and surface area be increased at the same time.

In recent years, great progress has been made in the synthesis, modification and applications of 1D TiO_2 nanostructured materials and other semiconductor oxides. In this review, we first provided a detailed discussion on the crystal structure of TiO_2 and the latest development on the fabrication of 1D TiO_2 nanostructured materials. Then, we will look into some critical structure engineering strategies that give 1D TiO_2 nanostructured materials excellent properties. Lastly, the environmental and energy applications of 1D TiO_2 nanostructured materials are summarized. Special focus has been given to their use as photocatalyst, supercapacitors, solar cells and lithium battery electrode.

2. Crystal structure and synthesis of 1D TiO_2 nanomaterials

2.1 Crystal structure of TiO_2

TiO_2 exists naturally mainly in three crystalline phases: anatase (tetragonal, space group I41/amd), rutile (tetragonal, space group P42/mnm), and brookite (orthorhombic, space group Pbca) (Figure 1a-c). In all polymorphs, titanium cations are six-fold coordinated to oxygen anions, forming distorted TiO_6 octahedra. Anatase have corner sharing with TiO_6 octahedra and rutile joined by sharing the octahedral edges, while brookite have TiO_6 octahedra joined by sharing both the octahedral corner and the octahedral edges. Besides, both anatase and rutile have a tetragonal structure with a=0.536 nm and c=0.953 nm (anatase), a=0.459 nm and c=0.296 nm (rutile), respectively. While Brookite has an orthorhombic structure with a=0.915 nm, b=0.544 nm, and c=0.514 nm.[47] Among the different polymorphs, rutile is generally considered to be the most stable bulk phase, while at the nanoscale, anatase and brookite are considered to be more stable due to lower surface energy, although there are some arguments in literature.[48, 49] The crystal phases are affected by the experimental conditions (synthesis method, annealing temperature, pH, duration etc.) and different crystal phases affect the performance. In the Yang's work,[50] rutile, anatase, and brookite TiO_2 nanorods with specific exposed crystal facets have been obtained by a hydrothermal method using peroxide titanic acid solution of different pH values. When the pH was lower than 8, only rutile phase was found. When the pH was ranging from 8 to 10, brookite and rutile were present in the mixed phases. However, when the pH was higher than 10, brookite and rutile disappeared, and there only existed anatase phase. Alsawat et al. discussed the effect of annealing temperature on the crystal phases and the performances.[51] No obvious peak was observed in the XRD pattern of the TiO_2 nanotube arrays (TiO_2 NTAs) before annealing. Conversion of the amorphous TiO_2 NTAs into anatase began at around 250 °C. The relative intensity of the anatase peaks increased with annealing temperature raising from 250 to 650 °C. When annealed at 650 °C, the TiO_2 NTAs consisted of an anatase and rutile mixed phase, indicating that a part of the anatase phase changed into a rutile phase as the temperature increased. At 850 °C, the peak intensity of rutile increased, while the anatase decreased. Besides, the TiO_2 NTAs with appropriate ratio of anatase and rutile showed the best photoelectric properties. Mi et al. also proved the mixed phase of anatase and rutile showed higher photocatalytic performance than pure one-phase crystal structure.[52] Tay et al. synthesized two-phase anatase/brookite TiO_2 nanostructures via a simple hydrothermal method.[53] In comparison with highly crystalline pure brookite and P25, the two-phase anatase/brookite TiO_2 showed higher hydrogen production activity.

Besides anatase, rutile and brookite, there exists another crystal phase of pure TiO_2, TiO_2(B) (Figure 1d), which is usually synthesized by hydrothermal method. Although having the same chemical formula TiO_2, TiO_2(B) has a more open framework structure, a relatively low density and a larger specific capacity than other polymorphs. This has led to growing applications in the fields of energy conversions, such as photocatalysts, solar cells and lithuium batteries.[54-57] Its space group C2/m composed of only two TiO_6 octahedra, with adjacent sheets joined together by edge-sharing. Zheng et al. denoted TiO_2(B) as the an intermediate product in the calcination of titanate, following the transformation sequence of protonated titanate → TiO_2(B) → anatase TiO_2.[58] Besides, $M_xTi_yO_{x/2+2y}$ (M = H, Li, Na, K etc.)[59-62] is another formula crystal structure of nanotubular products from the alkaline hydrothermal treatment of TiO_2. This structure is the intermediate product of TiO_2 and its nanobelts, nanowires and nanorods structures tend to have good crystallinity after ion exchange or calcination.

Anatase and rutile are the most studied polymorphs of TiO_2 for solar driven applications such as photocatalysis, water splitting, and solar cells. However, the wide band gap of TiO_2 (anatase: 3.2 eV, rutile: 3.0 eV) and fast recombination of photogenerated electron-hole pairs limited its wide applications. Their properties can be further improved via doping or forming heterojunctions with other phases with favourable electronic coupling,[63-65] this will be described in detail in section 3.

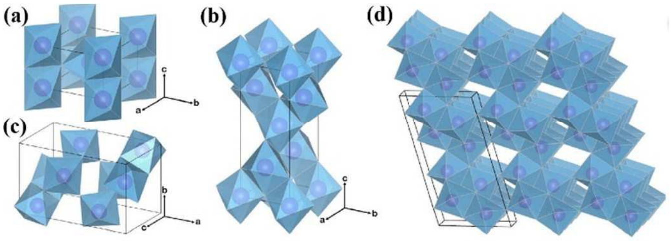

Figure 1. Crystal structures of TiO_2 polymorphs: Rutile (a), Anatase (b), Brookite (c) and TiO_2(B) (d). Purple spheres represent Ti atom, and the blue octahedra represent TiO_6 blocks. Oxygen atoms at the

corner of the octahedra are omitted for clarity. Reproduced from ref. 47. Copyright 2015 Royal Society of Chemistry.

2.2 Synthesis of 1D TiO_2 nanostructured materials

Many methods have been developed to prepare 1D TiO_2 nanostructures with various morphology, including nanotubes, nanorods, nanowires, nanobelts, nanosheets and nanofibers. In this section, we will briefly introduce six main preparation methods, hydrothermal, electrochemical anodization, vapor deposition, sol-gel, template-assisted, and electrospinning methods.

2.2.1 Hydrothermal method

The hydrothermal method is the mostly used for fabrication of 1D TiO_2 nanostructures. It is usually conducted in a stainless steel vessel with high temperature and pressure. Hydrothermal method has attracted much attention due to simple procedure and low production cost. Kasuga et al. firstly reported the fabrication of TiO_2-based nanotubular materials by hydrothermal method in 1998.[66, 67] In this process, amorphous TiO_2 powder was treated at high temperatures in a highly concentrated NaOH solution, and no sacrificial templates was needed. Since that, many investigations have been carried out on the synthesis of nanotubes,[68, 69] nanorods,[70, 71] nanowires,[72, 73] nanobelts[74, 75] nanosheets[76, 77] using hydrothermal method, as shown in Figure 2. Obviously, the hydrothermal synthesis of 1D TiO_2 nanostructures is a well-established technique and near 100% conversion of the precursors to 1D TiO_2 nanostructured materials in one single process.

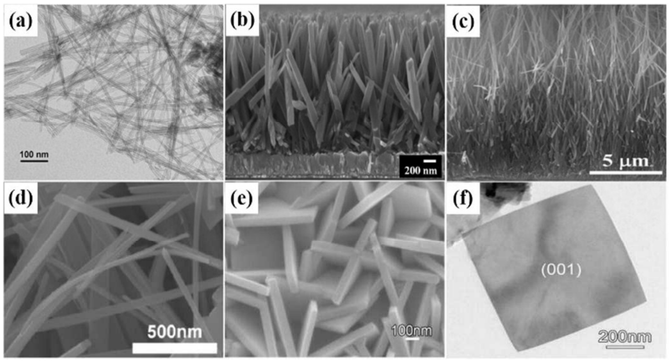

Figure 2. Different morphology types of 1D TiO_2 nanostructures synthesized by hydrothermal methods: (a) TiO_2 nanotubes, (b) TiO_2 nanorods, (c) TiO_2 nanowires, (d) TiO_2 nanobelts, (e,f) TiO_2 nanosheets. Reproduced from ref. 69. Copyright 2004 Royal Society of Chemistry (a). Reproduced from ref. 71. Copyright 2015 American Chemical Society (b). Reproduced from ref. 73. Copyright 2011 Royal Society of Chemistry (c). Reproduced from ref. 74. Copyright 2014 American Chemical Society (d). Reproduced from ref. 77. Copyright 2011 Wiley (e,f).

The synthesis method can be divided into the acid-hydrothermal and alkali-hydrothermal approaches according to the reactants used for the hydrothermal synthesis of 1D TiO_2 nanostructures.[78] In the former method, the reactants are usually titanium salts with hydrochloric acid. Reaction normally leads to the formation of TiO_2 nanorods. The reactants in the latter method are generally TiO_2 nanoparticles using sodium hydroxide solution. The dissolution-recrystallization is always involved in this process and the products include nanotubes, nanowires, nanobelts. These two methods have different reaction mechanisms, which produce different morphology and crystalline phases of the product in the 1D nanostructures.

It is evident that TiO_2 with different phase and morphology can be transformed to nanotubes under specific hydrothermal conditions. During hydrothermal process, layer-structured sodium titanate formed as an intermediate product on the surface of TiO_2 nanoparticles. Then, the Na^+ cations residing between the edge-shared TiO_6 octahedral layers can be replaced gradually by H_2O molecules. The size of intercalated H_2O molecules is larger than that of Na^+ ions, so the interlayer distance becomes enlarged, and the static interaction between neighboring TiO_6 octahedral sheets is weakened, causing the layered titanate particles exfoliate to form nanosheets. To release the high surface tension, the nanosheets curl up from the edges to form TiO_2 nanotubes.[79, 80] The dominant driving force for this curving process is still in discussion. Besides, hydrothermal conditions such as the type of precursor (TiO_2 nanoparticles or metal substrate), the type and concentration of the reaction solution, temperature, and time etc. have an important effect on the structures and morphologies of TiO_2. Morgan et al. investigated the concentration of NaOH solution and temperature on nanostructure formation from Degussa P25 through alkaline hydrothermal treatment.[81] As shown in Figure 3, different morphologies and structures of TiO_2 can be transferred from each other by adjusting the hydrothermal conditions. Besides, Tanaka and Peng et al. investigated the effect of concentration of NaOH solution, temperature and reaction time on nanostructure formation by using Ti substrate as precursor through alkaline hydrothermal treatment.[82, 83] Their results are consistent with the ones by Morgan's.

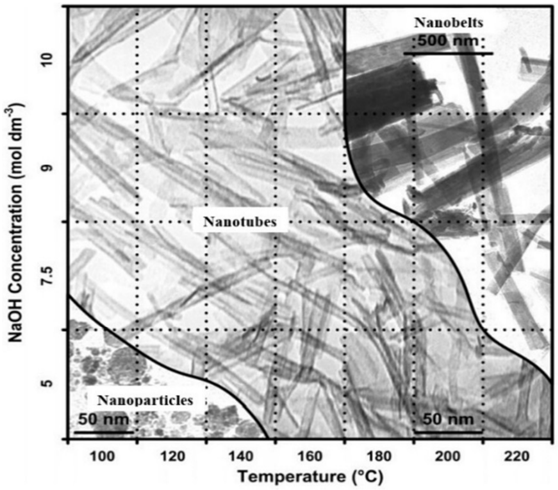

Figure 3. Morphological phase diagram of Degussa P25 evolution indicating regions of nanostructure formation after 20 h of hydrothermal treatment. Reproduced from ref. 81. Copyright 2008 American Chemical Society.

There are some disadvantages in the conventional hydrothermal method. First, slow reaction kinetics result in long reaction time. Second, short length of the nanotubes limits its wide applications. Third, nanotubes are non-uniform at large-scale. There, various approaches, such as ultrasonication-assisted, microwave-assisted, and rotation-assisted hydrothermal methods have been explored to solve these problems. Especially, Tang et al. grew elongated titanate nanotubes with length up to tens of micrometers by a stirring hydrothermal method (Figure 4),[84, 85] which has a major breakthrough on the development process of TiO_2 nanotubes. They obtained uniform nanotubes with high aspect ratio by optimizing the stirring rate. This method has resulted in 1D TiO_2-based nanotublar materials for long-life and ultrafast rechargeable lithium-ion batteries.

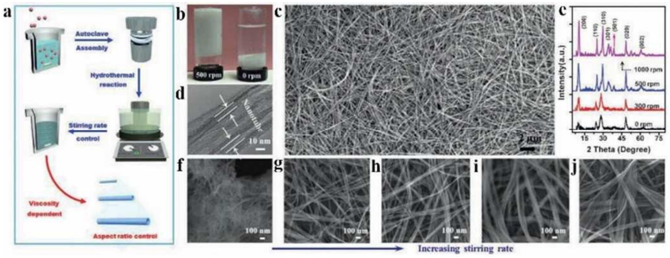

Figure 4. Fabrication and characterization of titanate nanotubes with different aspect ratios. a) Fabrication scheme. b) Digital photos of titanate solutions obtained by the stirring hydrothermal method at 500 (left) and 0 rpm (right) after sedimentation. c) FESEM images of titanate nanotubes obtained at 500 rpm. d) TEM image of c), the arrow indicates a nanotubular structure. e) XRD patterns of the products synthesized at different stirring speeds. f-j) FESEM images of the titanate nanotubes obtained by hydrothermal reaction at 130 °C for 24 h in at stirring rates of 0, 300, 400, 500, and 1000 rpm, respectively. Reproduced from ref. 84. Copyright 2014 Wiley.

2.2.2 Solvothermal method

The solvothermal method is also a common synthesis approach used for fabrication of 1D TiO_2 nanostructures.[86-88] It is similar to the hydrothermal method which is usually conducted in a stainless steel vessel with high temperature and pressure. In addition, these two methods both generally use TiO_2 nanoparticles, $TiCl_4$ or tetrabutyl titanate as the precursors. However, the solvothermal method is usually conducted in organic solvent (ethanol, ethylene glycol, n-hexane etc.), while the hydrothermal method usually reacts in water solutions.[89,90] Wang et al. synthesized a bundle of nanowires and open-ended TiO_2 nanotubes by solvothermal method using ethanol and glycerol as solvents, respectively (Figure 5a,b).[91] The obtained 1D TiO_2 nanostructures were found to exhibit a favourable discharge performance as anode materials in the application of lithium-ion batteries. What's more, anatase type nitrogen-fluorine (N-F) co-doped TiO_2 nanobelts were prepared by a facile one-step solvothermal method (Figure 5c). And the composites showed much higher photocatalytic degradation activity than TiO_2 nanoparticles.[92] Besides, Zhao's group successfully fabricated vertically aligned TiO_2 nanorods solvothermal method for preparing the photoanode in dye-sensitized solar cells and discussed the effect of thermal treatment on its performances (Figure 5d). It was found that the annealed TiO_2 nanorods showed increased power conversion due to improved crystallite.[93] Compared to hydrothermal method, how to choose the appropriate solvents is the key for the solvothermal method, which also limits its wide applications.

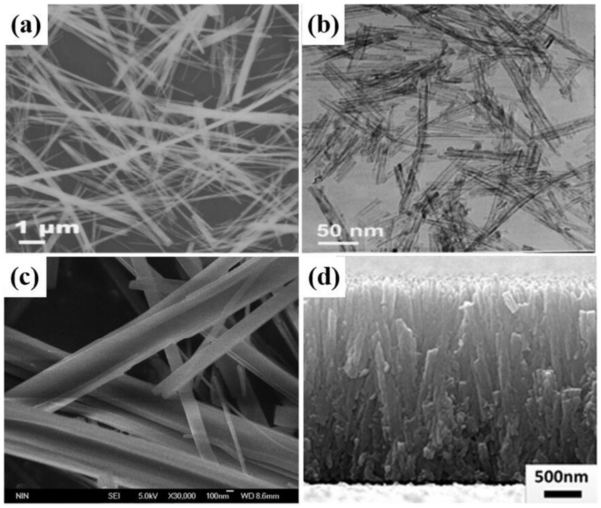

Figure 5. SEM images of various TiO_2 morphologies synthesized by solvothermal method: (a) nanowires, (b) nanotubes, (c) nanobelts, and (d) nanorods. Reproduced from ref. 91. Copyright 2006 American Chemical Society (a,b). Reproduced from ref. 92. Copyright 2012 American Chemical Society (c). Reproduced from ref. 93. Copyright 2014 Elsevier (d).

2.2.3 Electrochemical anodization method

1D TiO_2 nanotube arrays (TiO_2 NTAs) can be synthesized by a facile electrochemical anodization method on Ti metal substrate. Compared to other 1D TiO_2 nanostructured materials, TiO_2 NTAs are an excellent photoanode material that has been used for a long time because it is stable, non-toxic, environmentally friendly, inexpensive, recyclable and easily synthesized. The first report on anodized TiO_2 dates back to 1984, Assefpour-Dezfuly et al. produced porous TiO_2 by performing etching in alkaline peroxide firstly, and then followed by anodization in chromic acid.[94] As presented before, Zwilling and co-workers reported on the formation of nanoporous anodized titania in a fluoride containing electrolyte in 1999, making a breakthrough of work undertaken on porous/tubular anodized Ti over the last two decades.[95] Since then, much effort has been made to optimize experimental parameters with different electrolytes in order to efficiently achieve high quality self-organized TNAs. Categorized into 5 generations (Table 1 and Figure 6), highly ordered anodic TiO_2 nanotube arrays with long nanotubes have been realized, and the development is still ongoing. In general, the type of electrolyte, pH, applied potential, time and temperature affect the morphology and structure of TiO_2 NTAs. Hydrofluoric acid based water aqueous electrolytes is the most widely used in titanium anodization to produce TiO_2 nanostructures. However, the length of nanotubes is only a few hundred nanometers. In F^--based inorganic and organic neutral electrolytes, much longer and smoother nanotubes could be grown. The anodization voltage influences the morphology of formed nanostructures, while the anodization time mainly affects the length of TiO_2 nanotubes. The temperature of the electrolyte affects the dissolution rate. As a result, TiO_2 NTAs are normally grown at 20-25 °C (room temperature). Appropriate selection of anodization parameters for the TiO_2 NTAs fabrication is key to the successful growth of high quality nanotubes.

Table 1. Brief summary of various synthesis generations of TiO_2 TNAs.

TiO_2 NTAs	Electrolyte	Morphology	Ref.
1st generation (HF electrolyte)	0.5 wt% HF	Short nanotubes Length: 200-500 nm Diameter: 10-100 nm Wall thickness: 13-27 nm	95
2nd generation F^--based buffered electrolytes	1 M Na_2SO_4/$(NH_4)_2SO_4$ + 0.5 wt% NH_4F	Rough wall with wings Length: 0.5-2.4 μm Diameter: 100 nm Wall thickness: 12 nm	96
3rd generation Organic electrolytes containging F^-	0.5 wt% NH_4F + 2 v% H_2O in ethylene glycol	Smooth and ultra-long tubes Length: 5-1000 μm Diameter: 100 nm Wall thickness: 12 nm	97
4th generation Fluoride-free electrolytes	0.01-3 M $HClO_4$	Disordered tubes Length: 30 μm Diameter: 20-40 nm Wall thickness: 10 nm	98
5th generation Mutiple-step anodization in organic electrolytes containging F^-	0.5 wt% NH_4F + 2 v% H_2O in ethylene glycol	Smooth and hexagonal tubes Length: 2-10 μm Diameter: 100 nm Wall thickness: 15-20 nm	99,100

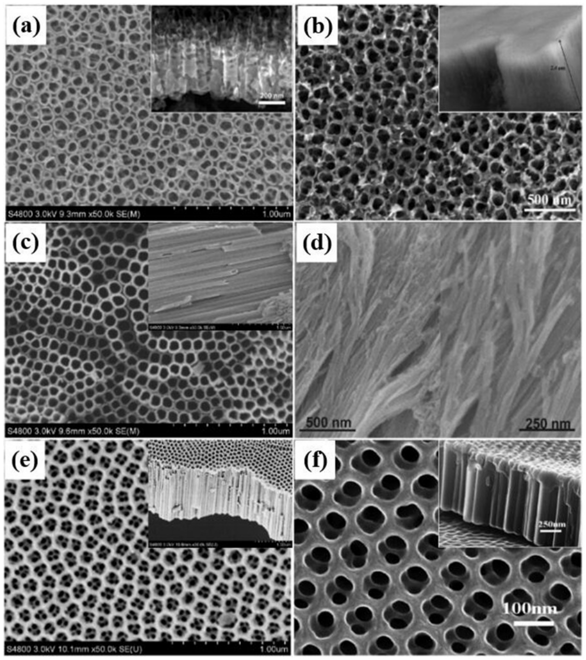

Figure 6. SEM images of 1st generation in HF electrolyte (a), 2nd generation in Na_2SO_4/NaF electrolyte (b), 3rd generation in ethylene glycol/fluoride electrolytes containing small amount of water (c), 4th generation in F^--free electrolyte (d), 5th generation with two-step anodization in ethylene glycol/fluoride electrolytes containing small amount of water (e) and 5th generation with three-step anodization in ethylene glycol/fluoride electrolytes containing small amount of water. Reproduced from ref. 95. Copyright 1999 Wiley (a). Reproduced from ref. 96. Copyright 2005 Elsevier (b). Reproduced from ref. 97. Copyright 2007 American Chemical Society (c). Reproduced from ref. 98. Copyright 2007 Elsevier (d). Reproduced from ref. 99. Copyright 2015 Royal Society of Chemistry (e). Reproduced from ref. 100. Copyright 2012 American Chemical Society (f).

2.2.4 Chemical vapor deposition method

The chemical vapor deposition (CVD) have been developed to construct high-quality 1D TiO_2 nanostructures. 1D TiO_2 nanostructures formed on silicon substrate coated with Ti, $TiCl_4$ or $Ti(OC_3H_7)_4$ in a sealed chamber with high temperature. Du et al. have grown uniform TiO_2 nanowires via the CVD method using $TiCl_4$ as the source reagent (Figure 7a).[101] Chen and Hoa et al. successfully synthesized nanorods and nanobelts by CVD method (Figure 7b,c).[102, 103] However, stringent experimental conditions and high cost put a limit to its wide production.

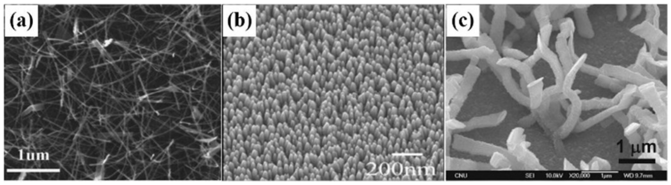

Figure 7. SEM images of nanowires (a), nanorods (b) and nanobelts (c) prepared by chemical vapor deposition. Reproduced from ref. 101. Copyright 2007 Elsevier (a). Reproduced from ref. 102. Copyright 2008 IOP Science (b). Reproduced from ref. 103. Copyright 2008 The Electrochemical Society (c).

2.2.5 Template-assisted method and sol-gel method

Template-assisted method is widely used in fabrication of 1D TiO_2 nanotubes and nanorods. Anodic aluminum oxide (AAO) nanoporous membrane, made of an array of parallel straight nanopores with controllable diameter and length, is usually used as a template. The template was removed by chemical etch after the TiO_2 was deposited into the template. Sander et al. fabricated dense and well-aligned of TiO_2 nanotubes with well-controlled dimensions by template-assisted method.[104] Sol-gel method is a representative of wet chemistry method to synthesize 1D TiO_2 nanostructures with low temperature and easy control of morphology. The general route to prepare TiO_2 sol gel is to mix tetrabutyl titanate or titanium isopropoxide in acetic acid. Then the solution is heated to high temperature with vigorous stirring to undergo hydrolysis and condensation reaction to obtain the nanostructured TiO_2. Joo et al. successfully synthesized TiO_2 nanorods with the diameter about 5 nm by sol-gel method.[105] Usually, 1D TiO_2-base nanostructures are constructed by the combination of the sol-gel and template-assisted processes. For example, as shown in Figure 7, Qiu, Attar and Lin et al. respectively fabricated 1D well-aligned TiO_2 nanotube arrays, nanorods and nanowires by a modified template-assisted sol-gel method (Figure 8a-c).[106-108] They can control the dimensions of TiO_2 nanostructures by through the template used.

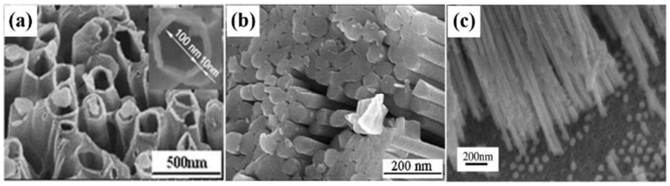

Figure 8. SEM images of TiO_2 nanotube arrays (a), nanorods (b) and nanowires (c) fabricated by template-assisted sol-gel method. Reproduced from ref. 106. Copyright 2006 IOP Science (a). Reproduced from ref. 107. Copyright 2009 Elsevier (b). Reproduced from ref. 108. Copyright 2003 IOP Science (c).

2.2.6 Electrospinning method

Since Li et al. firstly synthesized TiO_2 nanofibers with a diameter of 53 ± 8 nm by electrospinning method in 2003,[109] more and more researchers have paid attention to this simple method. During the electrospinning process, polymer solution is injected from a small nozzle under the influence of an electric field. The solution is then subjected to stretching by the continuous accumulation of electrostatic charges, forming ultralong and hollow nanofibers. Single-phase and high crystalline TiO_2 nanofibers can be obtained through calcination of the as-prepared samples. Yang et al. prepared TiO_2 nanofibers by using titanium tetraisopropoxide, acetic acid, ethanol and poly(vinyl pyrrolidone) (PVP) as starting materials.[110] As displayed in Figure 9, porous-shaped anatase TiO_2, cluster-shaped anatase TiO_2, hierarchical-shaped rutile (minor) TiO_2 and nano-necklace rutile (major) TiO_2 were achieved by annealing at different temperatures (500, 600, 700 and 800 °C). Along with the increased calcination temperature, the network structure and structural continuity of TiO_2 nanofibers are well maintained while the diameters of the as-synthesized TiO_2 nanofibers shrank from 200 nm to less than 100 nm. What's more, Ag, CuO and carbon etc. could be used to modify TiO_2 nanofibers by electrospinning to enhance photolytic activity.[111-113] Du's group synthesized coaxial electrospun TiO_2/ZnO core-sheath nanofibers by electrospinning method and this novel structure improved the overall energy conversion of dye-sensitized solar cells.[114]

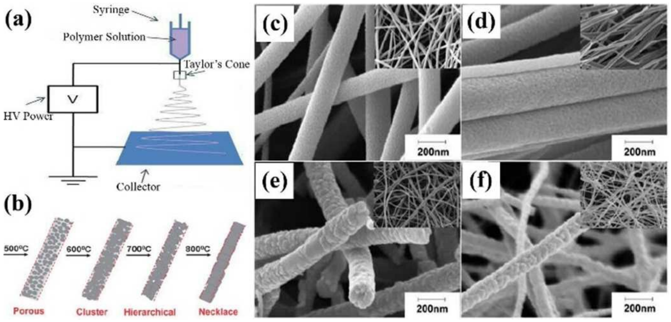

Figure 9. Schematic of the setup for electrospinning nanofibers (a). Schematic illustration of the morphology evolution mechanism from nanoporous to nanocluster, hierarchical and nanonecklace architectures of TiO_2 nanofibers (b). SEM images of TiO_2 nanofibers annealing at 500 °C (c), 600 °C (d), 700 °C (e) and 800 °C (f). Insets are the corresponding low-magnification views showing network-like and continuity of the nanofibers. Reproduced from ref. 110. Copyright 2013 Royal Society of Chemistry (c-f).

3. Surface engineering strategy

1D TiO_2 nanostructured materials have been widely employed in photocatalytic degradation of pollutants, water splitting, solar cells, supercapacitors, biomedical devices and lithium batteries due to its low-cost, good physical and chemical properties. However, 1D TiO_2 nanostructures show lower specific surface area when compared to 0D TiO_2 nanoparticles that can provide more photocatalytically active area. Besides, associated with wide band gap (anatase: 3.2 eV, rutile: 3.0 eV), TiO_2 can only absorb ultraviolet light (3-5% solar light), which hinders the full utilization of solar light. Single crystalline phase also leads to fast recombination of the electron/hole pairs. These drawbacks (low surface area, wide band gap, absorption UV light and single crystalline) make 1D TiO_2 inactive under visible light and limit it for a wider range of applications. Considerable efforts have been made over the past years towards enlarging the surface area, extending light absorption for visible light and suppressing recombination of photogenerated electron/holes.[115-117] The common strategies include increasing the specific surface area and materials modification via doping.

3.1 Enlargement of photocatalytically active area

Photocatalytic reactions occur at the active sites on the surface of a photocatalyst. Therefore, some important parameters such as specific surface area and high energy facets, which affect the efficiency of photocatalysis, should be taken into account for increasing the photolytic activity. These two factors will be discussed in the following subsections.

3.1.1 Enlargement of specific surface area

As we all know, the photocatalytic degradation of pollutants and photocatalytic water splitting occur on the surface (or near surface) of the photocatalysts. Therefore, it is important to create sufficient surface area to absorb the pollutants. Although 1D TiO_2 nanostructure has a unique surface and high aspect ratio, it has lower surface area when compared to 0D TiO_2 nanoparticles. There are two methods to enlarge the specific surface area. First, decorating second phase nanoparticles, nanorods or nanowires on the surface of 1D TiO_2 nanostructure has been proven beneficial to increase the specific surface area and absorption of pollutants. Besides, forming surface heterostructures can facilitate the separation of electron/ holes and improve the photocatalytic performances of the 1D nanostructure. However, it is difficult to control the size, distribution uniformity and density of the loaded nanoparticles, nanorods or nanowires on the 1D TiO_2 nanostructure. Second, construction of a coarse surface through a hydrothermal acid corrosion process can create numerous nanoparticles and pits on the surface of the existing 1D nanostructure. In addition, the acid corrosion method results in intimate contact between the in situ created nanoparticles and the 1D TiO_2 nanostructure, facilitating separation and transfer of photogenerated charges. Meng et al. successfully grew second phase TiO_2 nanorods with high density on TiO_2 nanofiber by electrospinning and hydrothermal method (Figure 10a-d).[118] The diameter and the length of these rutile nanorods could be varied from 10 nm to 400 nm and 20 nm to 1 μm, respectively, by changing the parameters of the hydrothermal reaction. The total surface area of the hierarchical nanostructures was doubled after the treatment. The photocatalytic activity of the TiO_2 hierarchical nanostructures was found to be superior to that of pure TiO_2 nanofibers due to the enlarged surface area and efficient separation of electron/holes. In another work, Wang and Zhou et al. created nanoparticles and pits on TiO_2 nanorods and nanotubes by HCl corrosion, respectively (Figure 10e-h). The modified 1D nanostructured materials showed higher photocatalytic degradation than the TiO_2 nanorods and nanotubes before the modification.[119, 120]

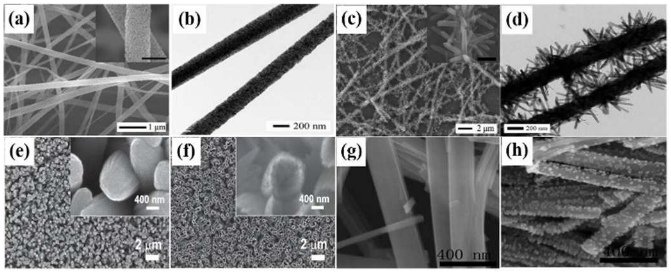

Figure 10. SEM and TEM images of pristine TiO_2 nanofibers (a,b) and TiO_2 hierarchical nanostructures (c,d). SEM images of pristine 1D TiO_2 nanorods and nanobelts (e,g). SEM images of 1D TiO_2 nanorods and nanobelts by HCl corrosion (f,h). Reproduced from ref. 118. Copyright 2011 Royal Society of Chemistry (a-d). Reproduced from ref. 119. Copyright 2015 Wiley (e,f). Reproduced from ref. 120. Copyright 2011 Royal Society of Chemistry (g,h).

3.1.2 Exposure of high-energy facets

Different facets of anatase TiO_2 were reported to possess different chemical properties, depending on the surface energy. The calculated surface formation energies of TiO_2 are 0.90 $J{\cdot}m^{-2}$ for the (001), 0.53 $J{\cdot}m^{-2}$ for the (100) and 0.44 $J{\cdot}m^{-2}$ for the (101) surface.[121] The higher surface energy of the (001) facets is due to the high densities of under-coordinated Ti atoms and the very large Ti-O-Ti bond angles at the surface.[122] Although the high-energy (001) facet exhibits highest photocatalytic activity, it is difficult to prepare (001) facet in 1D TiO_2 nanostructured materials because of its reduced stability. Zhang et al. reported that anatase nanorods with diameter around 10 nm were grown along the [001] direction, i.e., the c-axis of the anatase lattice, which has a minimum exposure of the high energy (001) surface.[123] Recently, the hydrothermal method was used to prepare TiO_2 structure with exposed (001) facets. Lu and co-workers made an important progress on preparation of anatase TiO_2 single crystals with exposed (001) facets. They synthesized anatase TiO_2 microcrystals with exposed (001) facets using TiF_4 as raw material via hydrothermal method.[124] Since then, more efforts have been put on preparing anatase TiO_2 single crystals with exposed (001) facets from different starting chemicals, such as titanium fluoride, titanium chloride, titanium tetrabutoxide, titanium tetraisopropoxide, and so on.[125-129] Wen's group synthesized large-sized well-defined anatase TiO_2 nanosheets wholly dominated with thermodynamically unfavourable high-reactive (001) and (100) facets (98.7% and 1.3%, respectively) by hydrothermal method.[130] The as-prepared anatase TiO_2 nanosheets show a well-faceted morphology and have a large size in length about 4.14 μm (Figure 11). These TiO_2 nanosheets with high percentage of (001) facets showed high photocatalytic activity. Besides, Yu et al. fabricated anatase TiO_2 nanosheets with exposed (001) facets by hydrothermal method and it showed higher photoelectric conversion efficiency in dye-sensitized solar cells than pure TiO_2 nanoparticles and P25.[131] In addition, the prepared TiO_2 nanosheet films electrode can be used in a wide range of applications including photocatalysis, electrochemistry, separation, and purification.

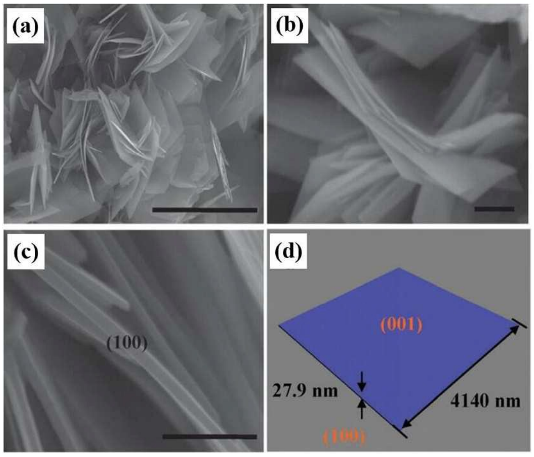

Figure 11. (a), (b) and (c) FESEM images of anatase TiO_2 nanosheets (d) Schematic structure of the as-obtained anatase TiO_2 nanosheets. Scale bars in (a-c) are 5.0 μm, 2.0 μm and 300 nm, respectively. Reproduced from ref. 130. Copyright 2011 Royal Society of Chemistry.

3.2 Modification strategy

TiO_2 is an n-type semiconductor with a wide band gap, and optical absorption in the UV region (<400 nm). Besides, the photogenerated electron and holes are easy to recombine for 0D, 1D, 2D TiO_2 nanostructures. Though compared to TiO_2 nanoparticles, the 1D nanostructure has superior charge transport through one dimensional direction, which should results in lower charge recombination in 1D TiO_2 nanostructure. It is still necessary to modify 1D TiO_2 nanostructured materials in the form of nanorods, nanotubes, nanowires and nanosheets, nanobelts and nanofibers with other materials to overcome these drawbacks. Numerous attempts toward achieving this goal have been made by employing various approaches including hydrothermal, sol-gel, thermal treatment, sputtering and electrochemical methods. Three essential benefits are expected: (1) doping with metal and non-metal elements to enhance light absorption and to prevent recombination of electron/holes, (2) loading metal nanoparticles to act as a surface plasmon resonance (SPR) photosensitizer for driving the visible light, (3) compositing with another semiconductor or conductor to form heterostructure that provides suitable energy levels for synergic absorption and charge separation for enhanced utilization of solar energy.

3.2.1 Doping with metal and non-metal elements

It is known that crystal structure and chemical composition affect the functionalities and performance of materials. Incorporating a secondary electronically active species into the lattice is able to sensitize 1D TiO_2 nanostructured materials for enhanced visible light absorption and suppressed recombination of electron and holes. Asahi et al. first reported that the nitrogen doped TiO_2 by sputtering in nitrogen-containing gas mixture and it showed extended absorption from UV light to visible light regions, leading to enhanced photocatalytic degradation of methylene orange (MO) under visible light irradiation.[132] Hou's group has conducted systematic investigation on N-doped TiO_2 nanotubes which were immersed in hot ammonia solution via hydrothermal method.[133] As displayed in Figure 12, it was found that the molar ratio between ammonia solution and deionized water had effect on the morphology on TiO_2 NTAs. Doping with nitrogen can effectively narrow the band gap of TiO_2 nanotubes and facilitate the transfer of photogenerated carries, dramatically enhancing photocatalytic activity for degradation of MO under visible light irradiation. Besides, other non-metals such as C,[134, 135] S,[136, 137] and F [138, 139] have also been introduced into TiO_2 lattice by various methods such as hydrothermal, sputtering and thermal treatment. Ion implantation or sputtering in an atmosphere of doping species followed by an annealing process has been verified to be an effective doping method.[140, 141] However, this method needs high energy accelerators in a high vacuum environment. Thermal treatment of 1D TiO_2 nanomaterials in special atmosphere and hydrothermal treatment are recognized as facile doping routes. Compared to bare TiO_2, non-metal doped TiO_2 exhibited a significantly improved photoresponse and higher photoelectron conversion efficiency. Among all the non-metal materials, carbon is also second mostly used (after nitrogen) to modify 1D TiO_2 nanostructured materials. Huo et al. constructed coaxial carbon/TiO_2 NTAs structure by hydrothermal treatment in a glucose solution and then carbonization under N_2 at 700 °C.[142] Besides, carbon quantum dots/titanium dioxide composite nanofibers were prepared via a facile one step hydrothermal method by Saud's group and it showed improved photocatalytic activity.[143] Graphene, a one-atom-thick sp^2-hybridized carbon material, has been widely used to modify TiO_2 due to its superior mechanical, electrical, and thermal properties.[134-137] Recently, our group has synthesized reduced graphene oxide/TiO_2 NTAs composite via a combination of electrodeposition and carbonation techniques.[99] In addition, Xiang et al. modified TiO_2 nanosheets with graphene by microwave-hydrothermal method.[138] The graphene/TiO_2 composite showed improved photocatalytic degradation of pollutants and photocatalytic hydrogen production activity under solar light. Though there exist a few reports on the modification of 1D TiO_2 nanomaterials with S and F, the existing literature is mainly focused on the co-doping of TiO_2 with N and F, or N and S.[144, 145] These results all demonstrated that doping with non-metal into TiO_2 lattice can enhance the light absorption and suppress the recombination of electron and holes, making TiO_2 more widely used.

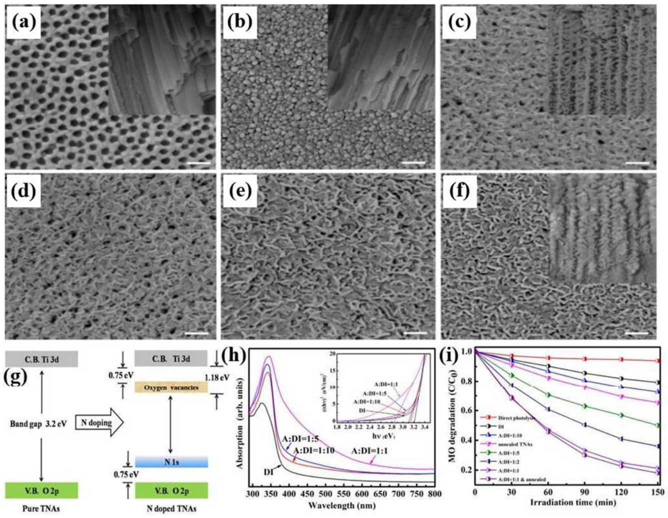

Figure 12. SEM images of images of as-anodized TiO_2 NTAs (a) after being immersed in water (b) and in ammonia solution (c-f, with the concentration of Vol (A):Vol (DI) = 1:10, 1:5, 1:2 and 1:1, respectively) by hydrothermal method. The bar scale is 200 nm. Schematic of the band structure of pure TiO_2 NTAs and N-doped TiO_2 NTAs (g). The absorption spectra of water immersed TNAs and different concentration nitrogen doped TiO_2 NTAs, the inset is the corresponding estimated bandgap (h). Photocatalytic degradation of MO under simulate visible light irradiation in the presence of photocatalysts (i). A and DI represent ammonia solution and deionized water, respectively. Reproduced from ref. 133. Copyright 2014 Elsevier.

At the same time, TiO_2 doped with transition metal cations such as Fe, V, Cu, and Mn have also been reported to enhance the photoelectron conversion efficiency under visible light illumination and suppress the recombination of photogenerated electron/hole pairs.[146-148] Su et al. incorporated Fe into TiO_2 nanotube arrays by an ultrasound-assisted impregnating-calcination method.[149] The Fe/TiO_2 NTAs sample showed excellent stability and improved photocatalytic degradation of acid orange Ⅱ with the synergistic effect of H_2O_2. It is noted that the performances of TiO_2 is largely dependent on the doping content, energy state, electron configuration and distribution. For example, when the doping content is excessively high, it may act as recombination centers, rather than facilitate electron-hole separation, resulting in decreased photocatalytic activity. Therefore, it is important to overcome these adverse effect by choosing the appropriate experimental parameters.

3.2.2 Loading with metal nanoparticles

Another promising approach is to decorate 1D TiO_2 nanostructured materials with noble metal nanoparticles (Au, Ag, Pt, Pd etc.).[150-153] Modification with noble metals has been proven to facilitate the transfer of photogenerated carriers and enhance photoelectron conversion efficiency under visible light. The Fermi level of some noble metals (Au, Ag and Pt etc.) is lower than the conduction band of TiO_2. Upon visible light illumination, the electrons transfer from the valance band of TiO_2 to the conduction band. Thus, noble metals act as the electron trap and the photogenerated electrons at the conduction band of TiO_2 will move towards the conduction band of noble metal. Simultaneously, the photogenerated holes transfer from the valence band of noble metal to that of TiO_2. Therefore, photogenerated electron-hole pairs are separated efficiently.[154, 155] Moreover, noble metal can also improve the photoresponse under visible light due to the surface plasmon resonance (SPR) effect.[156, 157] Many strategies have been adopted to decorate 1D TiO_2 nanomaterials with noble metal nanoparticles by UV irradiation reduction, plasma sputtering, electrodeposition, electrospinning and hydrothermal method. Among these methods, hydrothermal method exhibited better control of the metal particle size and dispersion. Ye and his colleagues sensitized TiO_2 NTAs with Pd quantum dots (Pd QDs/TiO_2 NTAs) via a facile hydrothermal strategy with superior performance in photoelectrocatalytic water splitting.[100] As shown in Figure 13a and Figure 13e, Pd quantum dots were uniformly dispersed over the entire surface of the nanotubes, both inside and outside of the nanotubes with very small particle size at 3.3 ± 0.7 nm. Besides, Lin et al. reported a facile hydrothermal strategy for crafting TiO_2 nanotubes sensitized by Pt nanoparticles by hydrothermal method (Figure 13b,f).[158] Pt nanoparticles with a diameter of 1.8 nm were tightly anchored on TiO_2 nanotubes and Pt nanoparticles effectively suppressed the recombination of electron/hole pairs, improving the photocatalytic hydrogen production activity. In addition, Ghaffari et al. adopted UV irradiation reduction method to construct highly dispersed Au nanoparticles on TiO_2 nanorods (Figure 13c,g).[159] Both the particle size and the amount of loading were facilely controlled via adjusting the concentration of $HAuCl_4$. The Au nanoparticles helped prevent photo injected electrons from approaching the surface of nanorods by forming a Schottky energy barrier, which improved the overall conversion efficiency of the dye-sensitized solar cells. Nam's group synthesized Ag/TiO_2 nanofibers composites via a one-step electrospinning process.[160] As depicted in Figure 13d and Figure 13h, Ag nanoparticles with the size of 8 nm were uniformly embedded on the surface of TiO_2 nanofibers. In comparison with the pristine 1D TiO_2 nanofibers, the specific capacity of Ag/TiO_2 nanofibers composites was increased by at least 20% because Ag nanoparticles promoted charge transfer and lithium-ion diffusion. 1D TiO_2 nanomaterials modified with noble metal can effectively prevent electron/hole recombination, facilitate the transfer of charge carriers and enhance visible light absorption, widening its applications in photocatalysis, solar cells, supercapacitors and lithium batteries.

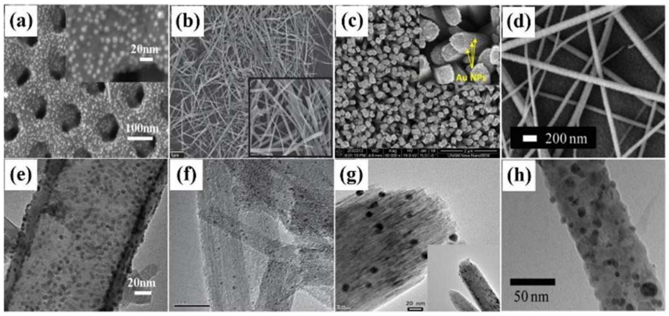

Figure 13. SEM images of Pd/TiO_2 NTAs (a), Pt/TiO_2 nanotubes (b), Au/TiO_2 nanorods (c) and Ag/TiO_2 nanofibers (d). (e), (f), (g) and (h) are the corresponding TEM images of (a), (b), (c) and (d). Reproduced from ref. 100. Copyright 2012 American Chemical Society (a,e). Reproduced from ref. 158. Copyright 2011 Royal Society of Chemistry (b,f). Reproduced from ref. 159. Copyright 2012 Elsevier (c,g). Reproduced from ref. 160. Copyright 2010 American Chemical Society (d,h).

3.2.3 Compositing with a semiconductor or conductor

It is proven an effectively strategy to incorporate a narrower band gap semiconductor (CdS, CdTe, PbS, Cu_2O etc.)[161-163] onto TiO_2 to form heterostructure for simultaneous visible light harvest and charge separation. Under visible light irradiation, photogenerated electrons are injected from the conduction band of the small band gap semiconductor to that of TiO_2, inhibiting the recombination of electron and holes. At the same time, the holes from the valance of TiO_2 will move to that of the semiconductor and then oxidize the targeted pollutants. Besides, semiconductor can facilitate the transfer of charge carriers under solar light, improving the overall power conversion efficiency of solar cells.

Cadmium sulfide (CdS) is a well-known semiconductor and widely used to couple with TiO_2. Its band gap is about 2.4 eV, matching well with the spectrum of sunlight, and able to absorb low energy photons up to 520 nm. Besides, its conduction band is more negative than TiO_2, facilitating the charge transfer across the interface between CdS and TiO_2. Electrochemical deposition and sequential chemical bath deposition (S-CBD) method are the conventional method to construct CdS/TiO_2 heterostructures. Shao et al. developed a constant current electrochemical deposition route to make CdS nanoparticles uniformly dispersed on the TiO_2 nanotubes and partially embed in the shell of TiO_2 nanotubes (Figure 14a,e).[164] The size and distribution density of CdS nanoparticles can be tuned easily by controlling the concentration of electrolyte. Coupling TiO_2 nanotubes with the CdS nanoparticles extended the optical absorption from ultraviolet into the visible-light region up to 580 nm. Compared with plain TiO_2 nanotube arrays, CdS/TiO_2 nanotube arrays showed an 11-fold enhancement in photoelectrochemical activity. This unique method is also suitable for the synthesis of other narrow band gap semiconductor-sensitized TiO_2 nanotubes. Kim's group fabricated CdS/TiO_2 nanowires by the S-CBD method.[165] First, TiO_2 nanowires was synthesized by hydrothermal method. Then, TiO_2 nanowires were immersed in Cd^{2+} and S^- solutions in sequence to uniformly deposit CdS nanoparticles with the size of 8 nm on the surface of TiO_2 nanowires (Figure 14b,f). Xie et al. decorated TiO_2 NTAs with CdS quantum dots (QDs) by a sonication-assisted sequential chemical bath deposition.[166] As shown in Figure 14c and Figure 14g, compared to the conventional S-CBD method, this method prevented CdS QDs from aggregating at the entrance of TiO_2 NTAs, and CdS QDs were uniformly dispersed both outside and inside TiO_2 nanotube surfaces. The CdS QDs/TiO_2 NTAs samples exhibited an enhanced photocurrent generation and photocatalytic efficiency under visible illumination due to efficient separation of photogenerated electron and holes. Liu et al. reported on a novel core-shell TiO_2 nanofiber/CdSe photoanode for photoelectrochemical hydrogen generation.[167] The core-shell nanofiber films, with a hierarchical network structure, are prepared on fluorine-doped tin oxide coated substrates via electrospinning pyrolysis and chemical bath deposition. CdS nanoparticles were uniformly dispersed on the of surface TiO_2 nanofiber (Figure 14d,h). The hierarchical network structure shows significantly improved photoelectrochemical properties due to the separation of charges. In addition, CdTe, CdSe and PbS are also widely used semiconductors. Rao's group co-sensitized vertically aligned anatase TiO_2 nanowire arrays with CdS/CdSe quantum dots (Figure 14i-l).[168] First, hierarchical TiO_2 nanowire arrays were synthesized by two-step hydrothermal. Then, CdS/CdSe quantum dots were uniformly deposited onto hierarchical TiO_2 nanowire arrays by electrodeposition. The hierarchical TiO_2 nanowire arrays based cell showed 30% higher power conversion efficiency than smooth TiO_2 nanowires devices duo to the superior light-scattering ability of branched hierarchical TiO_2 nanowires for enhanced light-harvesting efficiency and improved transfer of charge carriers in the existence of CdS and CdSe.

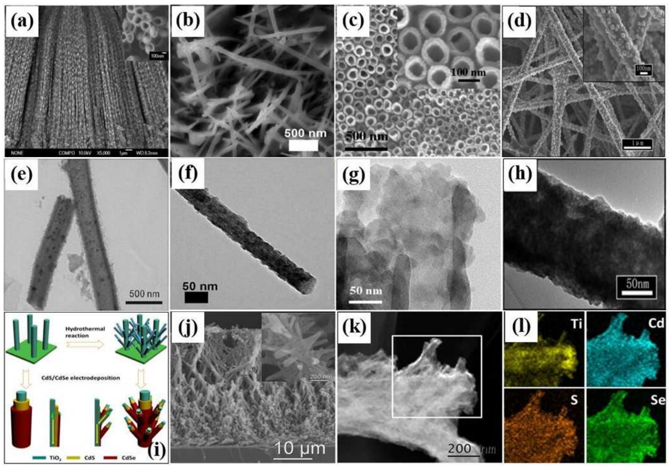

Figure 14. SEM images of CdS/TiO_2 nanotubes (a), CdS/TiO_2 nanowires (b), CdS/TiO_2 NTAs (c) and CdS/TiO_2 nanofibers (d). (e), (f), (g) and (h) are the corresponding TEM images. A schematic diagram showing the preparation process and structure of CdS/CdSe co-sensitized smooth and hierarchical TiO_2 nanowire (i), SEM image (j), HAADF-STEM (k) and EDX mappings (l) of CdS/CdSe/hierarchical TiO_2 nanowire photoanode. Reproduced from ref. 164. Copyright 2012 American Chemical Society (a,e). Reproduced from ref. 165. Copyright 2015 Elsevier (b,f). Reproduced from ref. 166. Copyright 2010 American Chemical Society (c,g). Reproduced from ref. 167. Copyright 2014 Royal Society of Chemistry (d,h). Reproduced from ref. 168. Copyright 2014 Elsevier (i-l).

Since TiO_2 is an n-type semiconductor, the construction of a p-n junction is believed to be one of the most effective strategies due to the existence of an internal electric field in the interface.[169-171] Wang et al. prepared Cu_2O/TiO_2 NTAs p-n heterojunction photoelectrodes via an ultrasonication-assisted sequential chemical bath method.[172] As displayed Figure 15a and Figure 15e, the Cu_2O nanoparticles were uniformly deposited on TiO_2 nanotubes. The amount of Cu_2O nanoparticles can be controlled by the deposition time. The p-n heterojunction effectively improved separation of photogenerated electrons/holes and enhanced the absorption of visible light. Compared to bare photocatalysis and electrocatalysis, Cu_2O/TiO_2 composite photoelectrodes also possessed superior photoelectrocatalytic activity and stability in rhodamine B (RhB) degradation with a synergistic effect between electricity and visible light irradiation. Besides, Deng et al. constructed p-n CuO/TiO_2 nanofiber heterostructure via a combination of electrospinning and hydrothermal strategies (Figure 15b,f).[173] It showed a high response and excellent selectivity to formaldehyde and ethanol gases because CuO can trap electrons and facilitate the charge transfer. In addition, decoration 1D TiO_2 nanomaterials with n-type semiconductor to form n-n heterojunction is also beneficial for improving the photocatalytic activity and power conversion efficiency. Ye et al. decorated n-type TiO_2 NTAs with n-type TiO_2 nanoparticles by hydrolysis of $TiCl_4$ solution, significantly increasing the surface area and improving the solar-cell efficiency (Figure 15c,g).[174] Besides, Yue's group synthesized n-n type TiO_2/ $CuInS_2$ nanorods core-shell heterostructure solar cell by solvothermal method (Figure 15d,h).[175] $CuInS_2/TiO_2$ nanorods showed much higher power conversion efficiency under solar light than pure TiO_2 nanorods due to the separation of electron and hole and the solar light harvest.

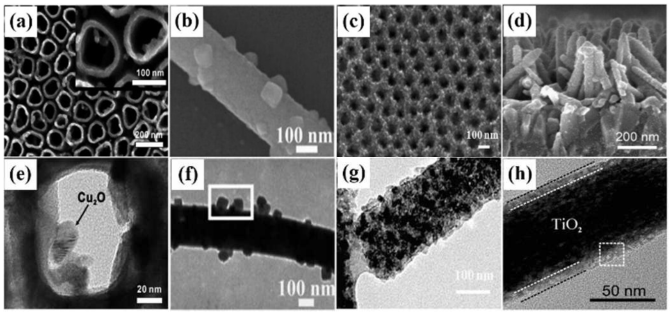

Figure 15. SEM images of Cu_2O/TiO_2NTAs (a),[172] CuO/TiO_2 nanofibers (b),[173] TiO_2 nanoparticles/TiO_2 NTAs (c)[174] and $CuInS_2/TiO_2$ nanorods (d).[175] (e), (f), (g) and (h) are the corresponding TEM images. Reproduced from ref. 172. Copyright 2013 Royal Society of Chemistry (a,e). Reproduced from ref. 173. Copyright 2014 Royal Society of Chemistry (b,f). Reproduced from ref. 174. Copyright 2011 American Chemical Society (c,g). Reproduced from ref. 175. Copyright 2015 Elsevier (d,h).

It is promising to construct perovskite ($BaTiO_3$, $SrTiO_3$, $CH_3NH_3PbI_3$, $CH_3NH_3PbCl_3$ etc.)/TiO_2 heterostructures for photocatalytic degradation of pollutants, photocatalytic water splitting and solar cells because perovskite can absorb solar light and facilitate the transfer of charge carriers. Huo's group prepared ordered perovskite-type $MTiO_3/TiO_2$ NTAs (M = Zn, Co, Ni) are by a general hydrothermal route based on amorphous TiO_2 NTAs via electrochemical anodization of Ti foil.[176] $MTiO_3/TiO_2$ NTAs showed good photocatalytic activity because perovskite can enhance the light absorption and effectively suppress the recombination of electro/holes. Meanwhile, Sun et al. modified TiO_2 NTAs with $SrTiO_3/TiO_2$ hetero-nanoparticles by two-step hydrothermal method.[177] Compared with pure TiO_2 NTAs or $SrTiO_3/TiO_2$ NTAs, TiO_2 NTAs modified with $SrTiO_3/TiO_2$ hetero-nanoparticles showed higher hydrogen production activity. Besides, Kim and his colleagues fabricated perovskite $CH_3NH_3PbI_3/TiO_2$ nanorods hybrids solar cell and a remarkable power conversion efficiency over 9.4 % was achieved based on the heterostructure.[178] Recently, perovskite materials coupling TiO_2 is a hot topic on photocatalysis, water splitting and solar cells due to its excellent performance.

Graphene, a two-dimensional carbon material with excellent electrical, mechanical and thermal properties, has been widely studied recently.[179-182] For example, Xiang et al. modified TiO_2 nanosheets with graphene by microwave-hydrothermal method.[183] The graphene/TiO_2 composite showed improved photocatalytic degradation of pollutants and photocatalytic hydrogen production activity under solar light. Besides, Perera's group prepared TiO_2 nanotube/reduced graphene oxide composites were prepared by an alkaline hydrothermal process. It was found that the ratio of RGO to TiO_2 in the composites significantly affects the photocatalytic activity. The composite with 10% RGO showed the highest photocatalytic activity, with a 3-fold enhancement in photocatalytic efficiency over pure TiO_2 nanotube both under UV light and visible light due to high surface area and efficient separation of electron/holes.[184] What's more, Pan et al. synthesized GO/TiO_2 nanowires and GO/TiO_2 nanoparticles by hydrothermal method. It was found that TiO_2 nanowires, in comparison with TiO_2 nanoparticles, have more uniform dispersion on graphene with less agglomeration, resulting in more direct contact between TiO_2 and graphene, and hence further improved electron-hole pairs separation and transportation. Therefore, the relative photocatalytic activity of GO/TiO_2 nanowires is much higher than GO/TiO_2 nanoparticles and pure TiO_2 nanowires or TiO_2 nanoparticles.[185]

4. Applications of 1D TiO_2 nanostructured materials

As described in Section 2, various kinds of 1D TiO_2 nanostructures have been fabricated using different effective methods. Owing to their excellent ion-exchange/intercalation activities, as well as adsorption/photocatalytic properties, 1D TiO_2 nanostructured materials have been paid much attention on photocatalytic degradation of pollutants, photocatalytic CO_2 reduction into energy fuels, photocatalytic water splitting, solar cells, supercapacitors and lithium batteries. In this section, we will discuss the various applications of 1D TiO_2 nanostructured materials in detail.

4.1 Photocatalytic application

TiO_2 nanostructured materials are widely used as photocatalysts due to its high oxidation and reduction ability. Whether aqueous pollutants or air pollutants, TiO_2 shows good photocatalytic activity. Besides, TiO_2 also displays good photoreduction activity of CO_2 into hydrocarbon energy fuels.

4.1.1 Photo/photoelectron-catalytic degradation of aqueous pollutants

With the fast development of economy, the environmental problems become more and more serious, especially clean water reduction and water contamination. Human beings urgently need effective solutions for these problems. TiO_2 has shown to be an excellent photocatalyst due to low-cost, non-toxicity, long-term stability and a strong oxidizing power to be useful for the decomposition of unwanted organic compounds. Upon UV illumination, the electrons at the valance band transfer to the conduction band by photon energy. The electrons at the conduction band can attack oxygen molecule to generate peroxide anion, and holes at the valance band can react with water to generate hydroxyl radicals at the same time, resulting in degrading pollutants (Figure 16a). Compared to photocatalysis, photoelectrocatalysis has showed higher photocatalytic degradation efficiency of pollutants. As depicted in Figure 16b, when a low bias potential was applied on the 1D TiO_2 nanostructures, it significantly facilitated the transfer of photocarriers and suppressed the recombination of photogenerated electrons and holes. Upon UV light irradiation, the electrons can leap up the valance band of TiO_2 to the conduction band, and then driven to the counter electrode via the external circuit, left the holes on the surface of the TiO_2 NTAs electrode. Meanwhile, a large number of active species were produced for pollutants degradation, following similar mechanisms for photocatalysis. Photocatalysis is mostly used for degradation of pollutants which is suitable for any form of TiO_2, while photoelectrocatalysis is more efficient and promising degradation strategy which needs 1D TiO_2 nanostructured materials (nanotubes, nanorods, nanowires, nanobelts and nanofibers) grown on Ti or FTO substrate.

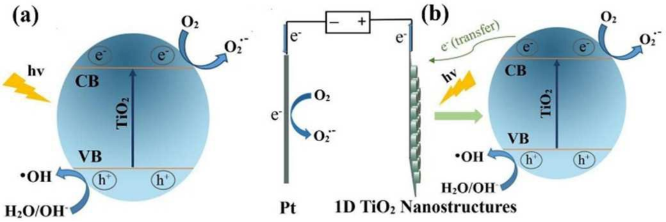

Figure 16. Mechanism of photocatalytic (a) and photoelectrocatalytic (b) degradation of pollutants for 1D TiO_2 photocatalysts.

Alsawat and Lai et al. studied the structures factors on the photocatalysis of TiO_2 nanotube arrays and demonstrated it had strong photocatalytic activity under UV light.[51, 186] Wang et al. synthesized cellulose acetate/TiO_2 ultrafine fibers via electrospinning for effective dyeing water treatment under UV light.[187] However, as discussed before, due to wide band gap and low solar light absorption, it is essential to couple 1D TiO_2 with metal, nonmetal and semiconductors to narrow the band and enhance visible light absorption for improved photocatalytic and photoelectrocatalytic activity. Yang et al. prepared Ag/TiO_2 nanotubes composite by a facile method.[188] Ag nanocrystals about 3.8 nm in diameter were uniformly distributed over the TiO_2 nanotubes surface (Figure 17a, b). The Ag/TiO_2 nanotubes composite exhibited the higher visible-light photocatalytic activity of rhodamine B (RhB) than P25 and TiO_2 nanotubes, which can almost degrade 100% RhB within 2 h due to the surface plasmon resonance (SPR) of Ag nanocrystals for enhanced visible light absorption and the high adsorption capability of TiO_2 nanotubes with large specific surface area (Figure 17c-d). Besides, TiO_2@carbon core/shell nanofibers (TiO_2@C NFs) with different thickness of carbon layers were fabricated by combining the electrospinning technique and hydrothermal method.[189] By adjusting the hydrothermal fabrication parameters, the thickness of carbon layer could be easily controlled from 2 to 8 nm. Furthermore, the TiO_2@C NFs exhibited enhanced photocatalytic efficiency of photodegradation of RhB compared with the pure TiO_2 nanofibers under visible light irradiation, which might be attributed to high separation efficiency of photogenerated electrons and holes based on the synergistic effect between carbon as a sensitizer and TiO_2 with 1D structure. The TiO_2@C NFs with 2 nm thick carbon layer showed higher photocatalytic activity than that with 8 nm on TiO_2@C NFs (Figure 17e-h). Notably, the TiO_2@C NFs could be easily recycled due to their one-dimensional nanostructural property. In addition, Zhang et al. constructed p-n Cu_2O/TiO_2 NTAs heterostructure by electrodeposition method. When compared with pure TNAs, the Cu_2O/TiO_2 heterojunction composites exhibit considerably higher photocurrent density and enhanced photoelectrocatalytic activity for the visible light driven photodegradation of methyl orange. Moreover, Cu_2O/TiO_2 NTAs composite photoelectrodes also possessed superior photoelectrocatalytic activity than photocatalytic performance. Recently, Zhang et al. prepared Cu_2O/TiO_2 NTAs p-n heterojunction photoelectrodes by electrodeposition method (Figure 18).[190] The Cu_2O nanoparticles were uniformly deposited on TiO_2 nanotubes. The electric field caused by p-n heterojunction effectively improved separation of photogenerated electrons and holes and enhanced the absorption of visible light. Consequently, Cu_2O/TiO_2 NTAs photoelectrodes exhibited a more effective photoconversion capability than single TiO_2 nanotubes. Furthermore, compared to bare photocatalyst, Cu_2O/TiO_2 composite photoelectrodes also possessed superior photoelectrocatalytic activity and stability in RhB degradation with a synergistic effect between electricity and visible light irradiation.

In addition to photocatalytic degrade the organic pollutants, the TiO_2 photocatalysts is also reported to effectively absorb and photocatalytic reduce various toxic metal ions, such as Hg(II), As(V), Cd(II) and Cr(VI), into less toxic metallic or ion state. For example, Liu's group synthesized TiO_2 nanotubes and displayed high photocatalytic reduction activity of Cr(VI) and Cr(III) in contaminated water.[191] In addition, Lu et al. decorated TiO_2 nanosheets with Mn_xO_y nanoparticles via a facile one-pot hydrothermal method. The composites displayed high photocatalytic degradation activity of Cr under visible light irradiation.[192] What's more, TiO_2 nanomaterials coupled with Au, N, CdS etc. also showed enhanced visible light photocatalytic and photoelectrocatalytic activity due to separation of electron/holes and solar light harvest.[193-195] Great efforts should be put on the modification of 1D TiO_2 nanostructured materials for improving the photocatalytic and photoelectrocatalytic degradation of pollutants in the future.

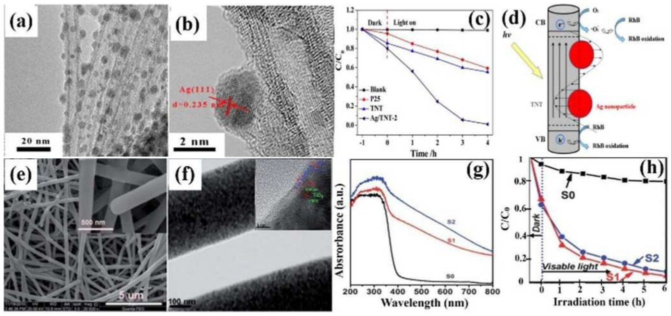

Figure 17. TEM images of Ag/TiO_2 nanotubes (a,b). Visible-light photocatalytic degradation curves of rhodamine B over P25, TiO_2 nanotubes, and Ag/TiO_2 nanotubes (c). Schematic illustration of the photocatalytic degradation mechanism of rhodamine B over the Ag/TiO_2 nanotubes under visible light (d). SEM images (e) and TEM images (f) of S2. UV-Vis diffuse reflectance spectra of the S0, S1 and S2 (g). Degradation profiles of rhodamine B over different samples (h). (S0: Pure TiO_2 nanofibers. S1, S2: TiO_2@C nanofibers with thickness of carbon layer about 2 and 8 nm, respectively.) Reproduced from ref. 188. Copyright 2015 American Chemical Society (a-d). Reproduced from ref. 189. Copyright 2011 Royal Society of Chemistry (e-h).

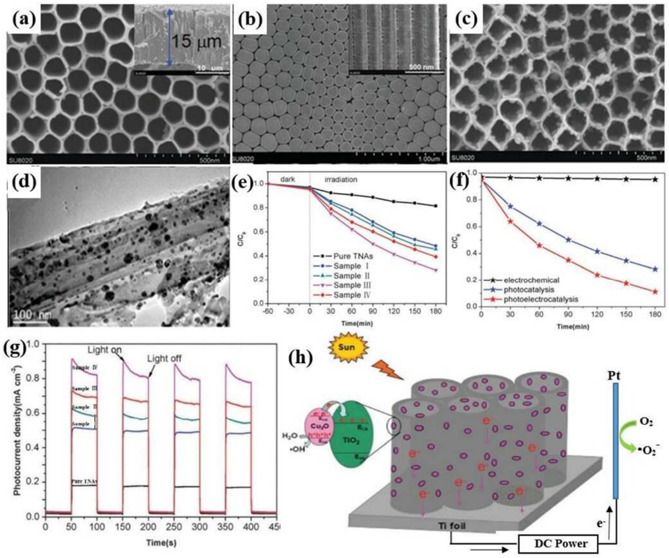

Figure 18. SEM images of pure TiO_2 NTAs (a,b). SEM image (c) and TEM image (d) of Cu_2O/TiO_2 NTAs with the deposition potential at -1.0 V. Photoelectrocatalytic activities of pure TiO_2 NTAs and sample I-IV toward the degradation of MO at an applied potential of 0.5 V (vs. Ag/AgCl) under visible light irradiation (e). Comparison of the electrochemical, photocatalytic and photoelectrocatalytic activities towards the degradation of MO for sample Ⅲ (f). Photocurrent response of pure TiO_2 NTAs and sample I-IV at the bias potential of 0 V (vs. Ag/AgCl) (g). The schematic diagram of the photoelectrocatalytic mechanism of Cu_2O/TiO_2 TNAs heterojunction composite (h). (Sample I-IV: Cu_2O/TiO_2 NTAs with the deposition potential at -0.8, -0.9, -1.0 and -1.2 V, respectively.) Reproduced from ref. 190. Copyright 2014 Royal Society of Chemistry (a-h).

4.1.2 Photocatalytic degradation of air pollutants

Indoor and outdoor air pollutants caused by factories, cars, new furniture, cooking etc. have increased much more day by day. This problem threated human being's health and lives seriously. And researchers paid much attention on dealing with it. Photocatalytic technology is considered as one of the potentially very efficient advanced oxidation and reduction processes for the improvement of the air quality by degrading inorganic and organic air pollutants.[196-199] Among semiconductors, TiO_2 is the most widely used in photocatalytic degradation of air pollutants due to low-cost, physical and chemical stability.[200-202] Compared to TiO_2 nanoparticles, 1D TiO_2 nanostructures are also widely used in photocatalytic degradation of air pollutants owing to large specific surface area and low recombination of electron/holes.[203,204] Nguyen et al. synthesized TiO_2 nanotubes by hydrothermal and discussed the washing pH on the photocatalytic oxidations of NO_x (NO, NO_2) which are linked to many environmental issues and considered as criteria pollutants in many countries.[205] It was found that the TiO_2 nanotubes washed at pH from 3 to 5 provided the highest efficiencies for total NO_x removal, which may be attributed to the synergistic effect of optimum conditions of sodium content, surface area, and amount of crystalline anatase achieved at these washing conditions (Figure 19a-c). Besides, Yu's group firstly prepared TiO_2 nanowires by a hydrothermal method and then calcined on various temperatures.[206] At a calcination temperature range of 400-600 °C, the TiO_2 nanowires showed higher photocatalytic activity than P25 powders for photocatalytic oxidation of acetone. Especially, at 500 °C, the calcined H-titanate nanowires showed the highest photocatalytic activity, which exceeded that of P25 by a factor of about 1.8 times. This can be attributed to the synergetic effect of larger specific surface area, higher pore volume and the presence of brookite TiO_2. In addition, Ren et al. studied the effect of the interaction between reactants and F-free or F-modified anatase TiO_2 nanosheets on photodegradation of volatile organic compounds such as acetone, benzene, and toluene.[207] The surface modification of TiO_2 nanosheets with F increases the interaction with acetone as compared to F-free TiO_2 nanosheets, resulting in the higher visible photocatalytic activity of the acetone. While F-free TiO_2 nanosheets exhibited higher visible photocatalytic activity of benzene or toluene due to the more strong interaction. The findings provide fundamental insight into the effect of the interaction, and open up a novel strategy for considerably enhancing photocatalytic efficiency and developing visible photocatalysis for environmental cleanup or selective purification through controlling the interaction. In order to improve the photocatalytic activity, Tang et al. reported the synthesis of 1D composites of titanate nanotube and carbon nanotube (denoted as TNT-CNT) by hydrothermal method (Figure 19d-f).[208] The titanate nanotube and carbon nanotube kept tubular morphology well and uniformly dispersed. By using of the degradation of benzene in the gas phase as a testing reaction, doping with carbon nanotube exhibited enhanced phototcatalytic performances than pristine TiO_2 nanotubes and TiO_2 nanoparticles, which could be an interesting research topic regarding TiO_2-carbon composites as photocatalyst for environmental remediation.

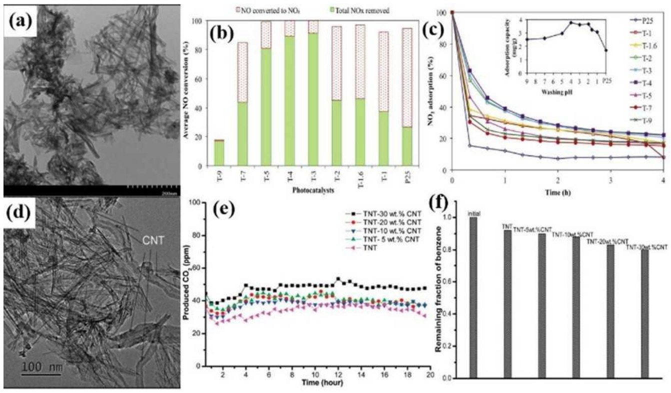

Figure 19. SEM image of TiO_2 nanotubes (a). Photocatalytic NO conversion and NO_x removal efficiency by TiO_2 nanotube with different washing pH, respectively (b,c).[205] Typical TEM images of TNT-30 wt% CNT (d). Time-online data for gas-phase photocatalytic degradation of benzene over the samples of TNT, and composites of TNT-CNT (e). The remaining fraction of benzene in the dark over the TNT and TNT-CNT nanocomposites after reaching the adsorption equilibrium for gas-phase degradation of benzene (f).[208] Reproduced from ref. 205. Copyright 2015 Elsevier (a-c). Reproduced from ref. 208. Copyright 2011 American Chemical Society (d-f).

4.1.3 Photocatalytic CO_2 reduction into energy fuels

With the rapid consumption of fossil fuels, the problem of global warming caused by the increase in the atmospheric concentration of CO_2 has raised public concern and research attention. Photocatalytic CO_2 reduction into hydrocarbon energy fuels is a promising and meaningful strategy which can both reduce the concentration of CO_2 and relieve the shortage of energy.[209-212] Since the discovery of photoreduction of CO_2 in semiconductor aqueous by Inoue's group,[213] tremendous endeavor has been put into synthesizing more effective and environmentally friendly photocatalysts to achieve CO_2 conversion more economically. As compared to other semiconductors, TiO_2 has been widely applied in photoreduction of CO_2 into energy fuels due to strong reduction ability.[214-217] As photocatalysts, the electrons at the valance band of TiO_2 transfer to the conduction band upon light illumination. The holes at the valance band can react with water to generate hydrogen ions, while the electrons at the conduction band can reduce CO_2 into energy fuels such as CH_4, CO, CH_3OH etc. at the same time, providing clear energy for the sustainable development (Figure 20a).[218-219] In the early stage, TiO_2 nanoparticles were firstly investigated for photocatalytic reduction of CO_2 due to large surface area, high porosity and chemical stability. Tseng et al. synthesized TiO_2 nanoparticles and Cu/TiO_2 nanoparticles composites by sol-gel method and compared their photoreduction rate with P25.[220] The methanol yield of Cu/TiO_2 was 20 $\mu mol \cdot g^{-1} \cdot h^{-1}$ under UV illumination. The yield was much higher than those of sol-gel TiO_2 and Degussa P25, whose yields were 0.8 and 6.4 $\mu mol \cdot g^{-1} \cdot h^{-1}$, respectively. Besides, Wang's group fabricated Pt/TiO_2 nanoparticles composites by photoreduction method.[221] For the optimized Pt/TiO_2 photocatalysts, the CH_4 yield reached 15 $mmol \cdot g^{-1} \cdot h^{-1}$, together with a H_2 yield of 22 $mmol \cdot g^{-1} \cdot h^{-1}$ and an

C_2H_6 yield of 0.7 mmol·g^{-1}·h^{-1} under visible light irradiation. The photocatalytic CO_2 conversion ability of Pt/TiO_2 was 3.7 times that of Pt/P25. In addition, noble metal (Pd, Pt, Au and Ag) modified reduced graphene oxide/TiO_2 nanoparticles ternary nanostructures are constructed for efficient visible-light-driven photoreduction of CO_2 into methane.[222] The photocatalytic activity of CO_2 reduction was found to follow the order: Pt/RGO/TiO_2 (0.28 μmol·g^{-1}·h^{-1}) > Pd/RGO/TiO_2 (0.20 μmol·g^{-1}·h^{-1}) > Ag/RGO/TiO_2 (0.17 μmol·g^{-1}·h^{-1}) > Au/RGO/TiO_2 (0.13 μmol·g^{-1}·h^{-1}) > RGO/TiO_2 (0.11 μmol·g^{-1}·h^{-1}) > P25 (0.02 μmol·g^{-1}·h^{-1}) under visible light irradiation. Except for 0D nanoparticles, 1D and 2D TiO_2 nanostructures are also applied in photocatalytic reduction of CO_2 due to large specific surface area (>50 m^2·g^{-1}) and slower recombination of electron/holes. Wang's group synthesized a unique one-dimensional structure of TiO_2 single crystals coated with ultrafine Pt nanoparticles (0.5-2.0 nm) via versatile gas-phase deposition methods.[223] The 1D TiO_2 film exhibited extremely higher CO_2 photoreduction efficiency with selective formation of methane (the maximum CH_4 yielding of 1361 μmol·g^{-1}·h^{-1}) than pristine P25.

Ping et al. fabricated TiO_2 nanotube arrays by electrochemical anodization and applied in photocatalyic reduction of CO_2 with H_2O into methanol and ethanol, and it showed higher photoreduction activity than TiO_2 nanoparticles.[224] In order to strengthen the visible light absorption and increase the photoreduction rate of CO_2, many effective strategies have been adopted to improve its performances. Feng et al. deposited ultrafine Pt nanoparticles on high aspect ratio nanotube arrays by using a rapid microwave-assisted solvothermal approach (Figure 20b).[225] The Pt nanoparticle were uniformly dispersed on the TiO_2 NTAs and the nanoparticle sizes can be controlled by adjusting the initial concentration of metal ion precursor inside the nanotube. The Pt/TiO_2 nanotube composite is shown to greatly promote the photocatalytic conversion of carbon dioxide and water vapor into methane, attributed to the homogeneous distribution of metal co-catalyst nanoparticles over the TiO_2 nanotube array surface providing a large number of active reduction sites and enhanced solar light absorption. This novel technique could prove useful for the deposition of metal, metal alloy, or metal oxide nanoparticles within a variety of nanotubular or nanoporous material systems with the resulting nanocomposites useful in catalysis, photocatalysis, photovoltaic, and photoelectrochemical applications. In addition, Varghese et al. synthesized nitrogen/TiO_2 nanotube arrays loaded with both Cu and Pt nanoparticles composites and discussed the annealing temperature on its photocatalytic reduction activity. And the composites annealed at 600 °C displayed highest hydrocarbon production rate of 111 ppm·cm^{-2}·h^{-1} under outdoor sunlight, which is at least 20 times higher than previous published reports (Figure 20c,d).[226] Besides, Xu et al. succeed in preparation of 2D anatase TiO_2 single crystals with marked photocatalytic activity via a facile and effective method.[227] The 2D TiO_2 nanosheets showed high photoreduction activity of CO_2 into CH_4 under solar light with large surface area (57.1 m^2·g^{-1}).

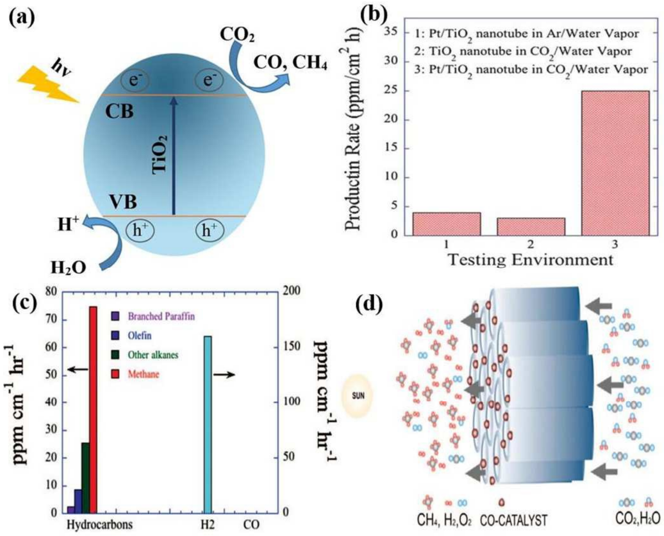

Figure 20. Mechanism of photocatalytic reduction of CO_2 for 1D TiO_2 photocatalysts (a). Methane production rates from bare TiO_2 NTAs and Pt/TiO_2 NTAs composite in carbon dioxide/water vapor and argon/water vapor environments (b). Product generation rates from a nitrogen-doped nanotube array film, 600 °C annealed, surface-loaded with both Pt and Cu catalysts (c). Depiction of co-catalyst loaded flow-through nanotube array membrane for high rate photocatalytic conversion of CO_2 and water vapor into hydrocarbon fuels (d). Reproduced from ref. 225. Copyright 2011 Royal Society of Chemistry (b). Reproduced from ref. 226. Copyright 2009 American Chemical Society (c,d).

4.2 Photo/photoelectron-catalytic water splitting

Faced with the challenge of fossil fuels reduction, human beings have urgently called on the sustainable energy economy. Since hydrogen was envisaged as a clean, renewable and abundant energy source, water splitting for hydrogen production by photocatalysts has become one of the efficient and promising ways to solve the problem of energy shortage in the future. Considering that the mechanism of photoelectrolytic water splitting is similar with photocatalytic degradation of pollutants (Figure 21), 1D nanostructured materials are considered as good candidates for high efficient water splitting. As for photocatalytic water splitting, the electrons at the conduction band can reduce H ions to generate hydrogen, and holes at the valance band can react with water to generate hydroxyl radicals at the same time, oxidizing pollutants (Figure 21a). Compared to photocatalysis, photoelectrocatalysis has showed higher degradation efficiency of pollutants. As displayed in Figure 21b, the electrons at the counter electrode and at the conduction band attack H ions to generate hydrogen, while the holes at the valance band can react with water to oxygen at the same time.

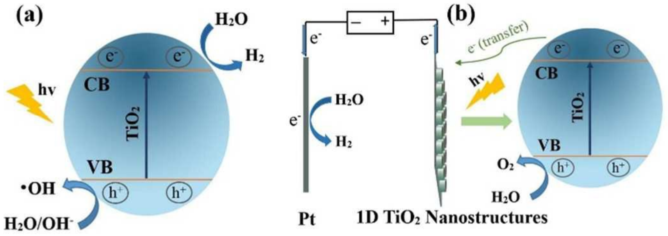

Figure 21. Mechanism of photocatalytic (a) and photoelectrocatalytic (b) water splitting for 1D TiO_2 photocatalysts.

TiO_2 nanomaterials showed high photocatalytic and photoelectrocatalytic water splitting under UV light. Meanwhile much efforts have been made into improving its performances by widening UV regions to visible light regions and suppressing the recombination of electron/holes (Table 2). Recently, Dang et al. reported a facile and green one-step hydrothermal method to prepare TiO_2 nanotube/graphene (TNT/GR) photocatalysts.[228] During hydrothermal reaction, the reduction of graphene oxide (GO) into GR without using any reducing agents and the formation of 1D TiO_2 nanotubes were achieved simultaneously, which resulted in the direct growth of well-defined TiO_2 nanotube uniformly distributed on GR substrates. TNT/GR nanocomposites with various GR contents (0.5, 1, 2, 5, 10 wt%) were prepared. The photocatalytic hydrogen generation was demonstrated under 300W Xenon lamp illumination with the light intensity about 60 mW·cm^{-2} by using methanol as sacrificial agent. A significantly enhanced photocatalytic hydrogen production (12.1 μmol·h^{-1}) was obtained over the composition-optimized TNT/GR composite (with 1.0 wt% GR), three times higher than that of pure TNT (4.0 μmol·h^{-1}) (Figure 22a-c). In addition, a plasmonic Ag/TiO_2 NTAs photocatalytic composite was designed for photoelectrocatalytic hydrogen evolution.[229] Ag quantum dots, with tunable size (1.3-21.0 nm), could be uniformly deposited on the TiO_2 NTAs by electrodeposition method. The unique structure of the as-obtained photoelectrodes greatly improved the photoelectric conversion efficiency. The as-obtained Ag/TiO_2 NTAs exhibited strong visible-light absorption capability, high photocurrent density, and enhanced photoelectrocatalytic (PEC) activity toward photoelectrocatalytic hydrogen evolution under visible-light irradiation (λ > 420 nm) (Figure 22d-h). The enhancement in the photoelectric conversion efficiency and activity was ascribed to the synergistic effects of silver and the unique hierarchical structures of TiO_2 nanotube arrays, strong SPR effect of Ag for enhanced visible light absorption. What's more, Mollavali's group firstly reported TiO_2 nanotube aligned arrays multiple-doped with nitrogen, nickel and carbon via a one-step anodization showed enhanced photoelectrocatalytic hydrogen production activity under visible light.[230] In general, the hydrogen production rate is greatly dependant on the electrolyte, external bias, light intensity, wavelength regions, and TiO_2 structures. Therefore, it is important to optimize these parameters based on fundamental understanding in order to design and construct high efficient cell for hydrogen generation.[231]

Table 2. Summary of TiO_2 based 1D nanomaterials in water splitting.

Photoanode	Light intensity (mW·cm^{-2})	Electrolyte	Photocatalysis/ photoelectrocatalysis	Water splitting efficiency	Ref.
TiO_2 NTAs	UV light 70 mW·cm^{-2}	1 M KOH	Photoelectrocatalysis	7.1 μmol·h^{-1}·cm^{-2}	232
TiO_2 NTAs	Solar light 150 W Xenon lamp	1 M NaOH	Photoelectrocatalysis	8.3 μmol·h^{-1}·cm^{-2}	233
Cu_2O/TiO_2 nanorods	Solar light	50% glycerol and 50% water	Photocatalysis	50.3 mmol·h^{-1}·g^{-1}	234
Ag/TiO_2 nanotubes	Visible light 100 mW·cm^{-2}	$MeOH/H_2O$ = 1:10	Photocatalysis	535 μmol·h^{-1}·g^{-1}	235
H/TiO_2 nanowires	UV light 100 mW·cm^{-2}	1 M NaOH	Photoelectrocatalysis	5.6 μmol·h^{-1}·cm^{-2}	236
Pt/TiO_2 NTAs	UV light 30 mW·cm^{-2}	0.1 M Na_2SO_4 and 1 M ethylene glycol	Photoelectrocatalysis	135 μmol·h^{-1}·cm^{-2}	237
Pt/TiO_2 NTAs	Solar light 320 mW·cm^{-2}	2 M Na_2CO_3 and 0.5 M ethylene glycol	Photoelectrocatalysis	492 μmol·h^{-1}·cm^{-2}	238
CdS/TiO_2 nanotubes	Solar light 300W Xenon lamp	0.25 M Na_2SO_3 and 0.35 M Na_2S	Photocatalysis	20 mmol·h^{-1}·g^{-1}	239
Graphene/CdS/ TiO_2 NTAs	Solar light 300 mW·cm^{-2}	0.1 M Na_2S and 0.1 M Na_2SO_3	Photoelectrocatalysis	10 μmol·h^{-1}·cm^{-2}	240
CdS/CdSe/TiO_2 NTAs	Solar light 100 mW·cm^{-2}	10% ethylene glycol and 0.1 M Na_2S	Photoelectrocatalysis	457 μmol·h^{-1}·cm^{-2}	241
$SrTiO_3/TiO_2$ NTAs	Solar light 320 mW·cm^{-2}	0.5 M KOH and 0.5 M ethylene glycol	Photoelectrocatalysis	314 μmol·h^{-1}·cm^{-2}	177
Pd/TiO_2 NTAs	Solar light 320 mW·cm^{-2}	2 M Na_2CO_3 and 0.5 M ethylene glycol	Photoelectrocatalysis	592 μmol·h^{-1}·cm^{-2}	100
C_3N_4/N/TiO_2 nanofibers	Solar light 300W Xenon lamp	10 mL methanol and 40 mL water	Photocatalysis	8391 μmol·h^{-1}·g^{-1}	242

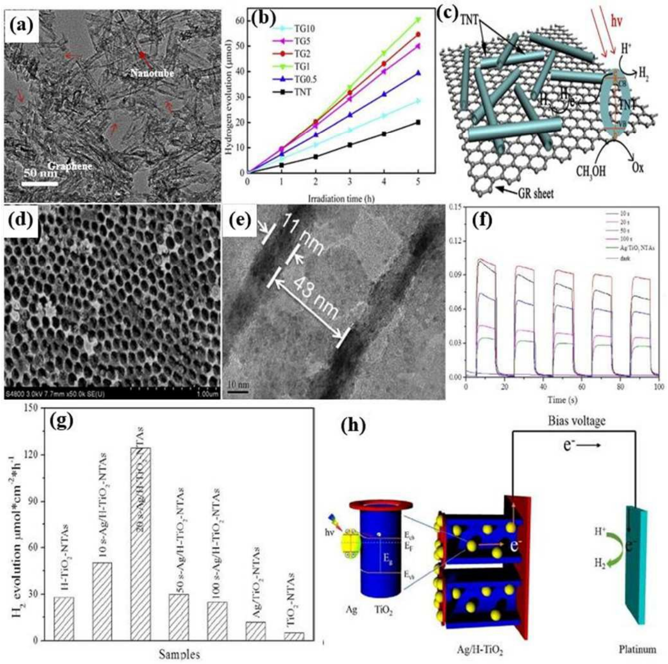

Figure 22. SEM image of graphene/TiO_2 nanotubes (a). Photocatalytic hydrogen production rate of pure TiO_2 nanotubes and graphene/TiO_2 nanotubes composites with various GR contents under solar light (b). Schematic diagram of charge transfer in graphene/TiO_2 nanotubes photocatalyst under Xe lamp irradiation (c). SEM (d) and TEM (e) image of pure TiO_2 NTAs and Ag/TiO_2 NTAs, respectively. Photocurrent (f) and photoelectrocatalytic hydrogen production rate (g) of pure TiO_2 nanotubes and Ag/TiO_2 NTAs with different deposition time at 0.7 V vs. SCE in a PEC cell containing a 2.0 M ethylene glycol and 0.5 M Na_2SO_4 solution under 300 W Xe lamp (> 420 nm filter) irradiation. SPR charge carrier transfer under visible light irradiation at Ag/TiO_2 NTAs interface and the photoelectrocatalytic process for H_2 evolution (h). Reproduced from ref. 228. Copyright 2013 Elsevier (a-c). Reproduced from ref. 229. Copyright 2015 Wiley (d-h).

4.3 Solar cells

One of the most promising applications of TiO_2 today is in solar cells, particularly dye-sensitized, quantum dots sensitized and perovskite solar cells.[243-247] For TiO_2 nanoparticles, the overall efficiency is limited due to electron loss during percolation through the nanoparticle network and photo-induced carrier recombination. Compared to TiO_2 nanoparticles, 1D TiO_2 nanostructures obtained high energy conversion efficiency due to high aspect ratio and facile transfer of electrons. However, it showed low photoelectric conversion efficiency under solar light due to the wide band and low utilization of solar light. Therefore, sensitized with organic dyes or inorganic narrow band gap semiconductors makes TiO_2 can absorb light into the visible region and convert solar energy into electrical energy.[248-250] These will be discussed in the following.

4.3.1 Dye-sensitized solar cells

The dye-sensitized solar cell (DSSC), a concept first introduced by O'Regan and Gratzel in 1991,[251] is widely studied for achieving the goal of high efficiency and low cost in the utilization of solar energy.[252-254] The working principle is displayed in Figure 23a. A typical configuration of DSSC exhibits a sandwich structure: a photoanode and counter electrode are placed in parallel and separated by an electrolyte. Transparent conducting substrate composed of nanocrystalline semiconductor (TiO_2 is most widely used) on one side served as photoanode. A catalytic layer such as platinum or carbon materials usually serves as the counter electrode. An adsorbed Ru-dye is used as a sensitizer and electrolyte. Upon illumination, the dye molecules capture photons and then inject electrons into the conduction band of the semiconductor. Electrons migrate through the semiconductor layer and travel through the external circuit. Then the oxidized dye is reduced to its original state by electron donation from the redox couple in the electrolyte. Usually the electrolyte is an organic solvent or ionic liquid containing the I^-/I^{3-} redox system. The I^{3-} loses electrons and is oxidized to I^- While the resulting I^- species can diffuse to the Pt counter electrode where they are regenerated to I^{3-} by reduction, regenerating the dye at the same time. During these process, charge injection and transport are always accompanied by charge recombination, which decays the output performances of the DSSC.[255, 256]

At early stage of the development, Ohsaki's group synthesized TiO_2 nanotubes by hydrothermal method and applied them for DSSC applications.[257] They studied the fabrication conditions (pH of paste, sintering temperature and the electrolyte) of TiO_2 nanotubes electrode that affect the performance of DSSCs. In comparison with commercially available nanoparticles P25, the DSSC using TiO_2 nanotubes electrode show higher energy conversion efficiency (6.4%) than that using P25 particle electrode (5.5%). The better performance was mainly due to the improved electron transfer with the tube structure. Shankar et al. fabricated long, vertically aligned TiO_2 nanotubes arrays with lengths between 10 and 220 μm by electrochemical anodization method. Dye sensitized solar cells containing these arrays yielded a power conversion efficiency of 6.89%.[258] In order to increase the overall conversion efficiency, surface modification and morphology design have been explored to enhance the electron transfer ability of 1D nanostructures. Plasmonic Ag and Au were used to decorate TiO_2 nanofibers to improve the conversion efficiency of DSSC, which reached 6.13% and 7.7% conversion efficiency, respectively.[259,260] Surface plasmon resonance of noble metals for visible light absorption, separation and better transfer of electrons were the contributing factors. Besides, TiO_2 nanotubes coupled with TiO_2 nanoparticles showed higher power conversion efficiency at more than 7.0%, which was a great progress on the conversion efficiency of 1D TiO_2 nanotubes.[261-263] Lv et al. reported that an optimized porous rutile TiO_2 nanorod arrays (NRAs) with a large internal surface area was fabricated on the FTO substrate via two-step hydrothermal treatment (Figure 23b-e).[264] The porous rutile TiO_2 NRAs with a large surface area achieved a record efficiency of 7.91% for the DSSC. Some researchers modify 1D TiO_2 nanostructures with carbon, ZnO etc. for improving photo conversion efficiency.[265-267] However, there exists several problems. The organic dyes are difficult to synthesize and the cost is high. Besides, limited photoelectric conversion efficiency has restricted the commercialization of DSSCs. However, with more interests and efforts put on the DSSC, these problems will eventually be overcome and the conversion efficiency will continue to improve in the future.

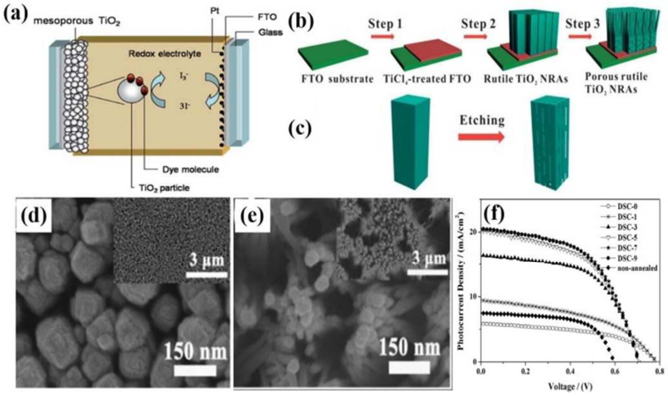

Figure 23. Schematic overview of a dye-sensitized solar cell (a). Processes of preparing 1-D porous rutile TiO_2 NRAs (b). Morphological development of single TiO_2 NRAs by step 3 (c). SEM image of pristine TiO_2 NRAs (d) and porous rutile TiO_2 NRAs (e). J-V characteristics of DSSC based on rutile TiO_2 NRAs with different etching duration and P25 TiO_2 nanoparticles film (g). Reproduced from ref. 255. Copyright 2010 American Chemical Society (a). Reproduced from ref. 264. Copyright 2013 American Chemical Society (b-f).

4.3.2 Quantum dots-sensitized solar cells

In pursuit of low-cost, easy fabrication, and environmentally friendly energy, photovoltaic cells converting solar energy to electricity is a promising strategy to address the energy crisis. Quantum dots-sensitized solar cells (QDSSC) have been more and more popular and are considered as promising alternatives to DSSCs due to higher light absorption, low-cost and long cycling stability.[268-270] As is shown in Figure 24A, the working principle of QDSSC is similar to that of DSSC. The classical architecture of a QDSSC consists of three components: TiO_2 sensitized quantum dots as photoanode, a counter electrode, and a redox electrolyte having S^{2-}/S_n^{2-} couples. Transparent conducting substrate composed of nanocrystalline semiconductor (TiO_2 is most widely used) on one side coated with another semiconductor quantum dots served as photoanode. A catalytic layer such as platinum or carbon materials usually serves as the counter electrode. The polysulfide serves as the electrolyte. Upon light irradiation, quantum dots can absorb photons and excite electrons from the valence band of quantum dots to their conduction band. Due to the good match of energy levels, electrons on the conduction band of quantum dots flow to that of TiO_2. And then the photoelectrons in the CB are collected by transparent conductive oxide, flow through the external circuit. Quantum dots are subsequently regenerated by reducing species in the electrolyte. Finally, holes are transported to the counter electrode, where the oxidized counterpart of the redox system is reduced. During this process, photogenerated electrons and holes are effectively separated.[271-273] In order to improve the photovoltaic performances of QDSSC, many researchers have focused their attention on materials selection and materials engineering. Quantum dots (CdS, CdSe, CdTe, PbS, carbon etc.) with size-dependent band gaps provide new opportunities for harvesting light ranging from the visible to the infrared regions of solar light. In addition, through the impact ionization effect, it is possible to generate multiple excitons from single-photon absorption in quantum dots.[274,275] As have been reported, these quantum dots can be easily deposited on the surface of 1D TiO_2 nanostructures at room temperature by successive ionic layer-by-layer adsorption and reaction (SILAR),[276] chemical bath deposition (CBD)[277,278] and electrodeposition method.[279] Sudhagar et al. prepared the CdS/CdSe coupled TiO_2 nanofibrous electrode with a maximum power conversion efficiency (PCE) of 2.69%, while Sun et al. reported a novel CdS quantum dots sensitized TiO_2 TNAs photoelectrodes by a sequential chemical bath deposition technique and the PCE of QDSSC efficiency increased up to 4.15% under solar light due to the fast and efficient transfer of the photogenerated electrons and enhanced light harvest (Figure 24B-D).[280] Recently, Chen et al. fabricated the ultralong TiO_2 nanorod arrays co-sensitized with CdS/CdSe quantum dots for QDSSC by a combination of SILAR and CBD method.[281] A thickness of 17.6 μm TiO_2 nanorod arrays with large inner surface area was first used for sandwich-type ordered QDSSC, it is found that the cell exhibited a greatly enhanced short-circuit current density and the conversion efficiency reached 2.66%. In addition, as described in section 3.2, Rao's group co-sensitized vertically aligned anatase TiO_2 nanowire arrays with CdS/CdSe quantum dots by electrodeposition and showed an impressive photovoltaic performance of 4.20%.[168] These results clearly demonstrate that the synergistic effect of unique nanotube structure and quantum dots can facilitate the propagation and kinetic separation of photogenerated charges. Besides, multiple-demensional hyperbranched ZnO/TiO_2 heterostructure arrays showed high efficiency around 6% for quantum dots sensitized solar cells.[282, 283] However, QDSSCs have not been demonstrated as efficient photovoltaic cells than expected and the reported PCE is lower than 10%. Therefore, great efforts are still needed to inhibit charge recombination at the semiconductor surface and to seek for an effective organic dye for the efficiency improvement.[284]

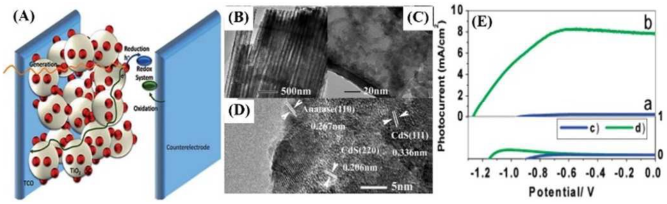

Figure 24. Schematic illustration of the structures of a typical QDSSC (A). TEM (B,C) and HRTEM (D) images of CdS/TiO_2 NTAs. Photocurrent versus voltage spectra (E) in 1 M Na_2S solution under solar light illumination for plain (a) and CdS quantum dots modified TiO_2 nanotube film electrode (b). (c,d) Corresponding currents in the dark for curves a and b. Reproduced from ref. 271. Copyright 2010 American Chemical Society (A). Reproduced from ref. 280. Copyright 2008 American Chemical Society (B-E).

4.3.3 Perovskite solar cells

Perovskite solar cells based on organometal halides represent an emerging photovoltaic technology with high photovoltaic performances over than 50% in theory, which have attracted much attention in recent years.[285-289] The mechanism of perovskite solar cells is displayed in Figure 25a. A relatively thin layer of mesoporous TiO_2 film is deposited on the top of a compact layer (as a blocking layer) on a transparent conductive oxide (TCO) glass substrate. Then an absorber layer is formed by adsorbing a monolayer of a sensitizer on the mesoporous TiO_2 layer, and the hole transporting material then infiltrates into the pores. As a result, a thin photoanode layer is a prerequisite to facilitate pore filling and to generate a suitable diffusion length to restrain charge recombination. Finally, a thin film of a metal (Au or Ag) counter electrode is deposited to collect the generated charges.[290] As a new member of the next generation photovoltaic materials, organometal halide perovskite was first demonstrated for efficient solar cells with the power conversion efficiency around 4% in 2009,[291] and soon become the most important candidate to replace silicon, with low material cost and high efficiency. Burschka's group made a biggest scientific breakthroughs on perovskite solar cells in 2013 and increased the PCE to 15%.[292] Up to now, perovskite solar cells have achieved a stunning success in a very short period in terms of efficiency owing to the high light absorption coefficient, effective separation and transfer of electrons. Among inorganic hybrid perovskites $CH_3NH_3PbX_3$ (X = Cl, Br, I), $CH_3NH_3PbI_3$ is mostly used to modify 1D TiO_2 nanostructures.[293-295] Recently, Wang's group successfully fabricated flexible, solid-state TiO_2 NTAs/$CH_3NH_3PbI_3$ perovskite solar cell.[296] The Ti foil/TNTs act as scaffold for perovskite loading and electron transport layer, while the transparent carbon nanotubes top electrode acts as hole collecting layer and light transmission. To date, the first attempt of Ti metal foil substrate based flexible perovskite solar cell with a decent power conversion efficiency of 8.31% has been achieved. Besides, Jiang et al. reported a solvothermal method for the synthesis of rutile TiO_2 nanowires with a controllable length-to-diameter ratio and well-separated wire-to-wire space.[297] They also demonstrated that electron transport in these rutile nanowires is 200 times faster than that of mesoporous rutile films. The $CH_3NH_3PbI_3/TiO_2$ nanowires perovskite solar cell with optimized length showed a higher photo conversion efficiency around 11.7%. What's more, a remarkable power conversion efficiency (PCE) around 10% was achieved based on the simple TiO_2 nanorod/$CH_3NH_3PbI_3$ hybrid perovskite solar cell (Figure 25b-d).[178,298,299] Since organometal halide perovskite solar cells are low-cost and have shown a higher PCE values over 15%, perovskite solar cells will continue to receive great amount of attention among the non-silicon based photovoltaic technology.

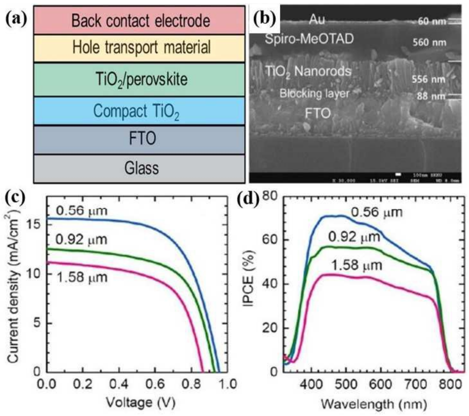

Figure 25. Schematic illustration of the structures of a typical perovskite solar cell (a). Cross-sectional SEM image of solid state TiO_2 nanorod/$CH_3NH_3PbI_3$ hybrid photoanode (b). Current density-voltage curves (c) and IPCE spectra (d) of TiO_2 nanorod/$CH_3NH_3PbI_3$ perovskite solar cell with different length of TiO_2 nanorod. Reproduced from ref. 290. Copyright 2015 Royal Society of Chemistry (b). Reproduced from ref. 178. Copyright 2013 American Chemical Society (b-d).

4.4 Lithium-ion batteries

Rechargeable lithium-ion batteries (LIBs) have attracted extensive attentions in recent years for their potential applications in consumer devices and electric vehicles due to high energy density and great longevity.[300-303] Similar to the architecture of basic Galvanic cells, a lithium-ion battery consists of three functional components: the anode, cathode, and electrolyte. As shown in Figure 26a, the basic operating principle of LIBs is based on Li^+ shuttling reaction between the anode and the cathode. When the battery is discharged, Li ions intercalate the positive materials and move from the anode to cathode through the electrolyte, while electrons flow through external circuits to provide electricity. During charging process, an external electrical power source forces the current to pass in the reverse direction and make lithium ions migrate from the cathode to the anode across the electrolyte. Therefore, the properties of the active Li storage materials greatly influence the capacitance and performance of rechargeable LIBs. Generally, larger number of Li ions accommodated in electrode materials leads to higher specific capacity of the battery. Besides, electrodes materials with open structure and short diffusion length allowing for fast ionic/electronic transfer can obtain high current density and high power density.[304, 305] Graphite as anode material has been used in majority commercial LIBs before. However, graphite electrode suffered from poor rate capacity, short cycle life, safety concerns, and poor low temperature performance. Therefore, it can't meet increasing demands of electric device and was replaced by transition metal oxides due to their excellent electrochemical properties.[306, 307] Among these materials, 1D TiO_2 nanostructures have been considered a promising candidate due to their open, mesoporous structure, good safety, efficient transport of lithium ions. Especially 1D TiO_2 nanotubes and nanowires have an open layered structure with a much larger interlayer spacing, making them good candidates to provide fast diffusion channels for reversible lithium ion intercalation and deintercalation, which results in a high value of charge/discharge capacity.[308-310] The overall lithiation reaction for TiO_2 nanomaterials is listed in equation (1):

$$xLi^+ + TiO_2 + xe^- \Longleftrightarrow Li_xTiO_2\ (0 \le x \le 1) \qquad (1)$$

Up to now, lithium-ion batteries with high specific capacity, high rate capacity, long-term stability and high safety have been obtained by using TiO_2 nanomaterials as anode materials. In terms of specific capacity, the earliest work by Armstrong et al. suggested that an initial discharge capacities of 230 $mA\cdot h\cdot g^{-1}$ at current densities of 50 $mA\cdot g^{-1}$ can be achieved by TiO_2(B) nanowires.[311] After that, TiO_2(B) nanowires have been attracted much interests duo to the lowed intensity than anatase, rutile and brookite which makes it an ideal host for Li^+ intercalation and hence the controlled introduction of Li^+ and electrons into TiO_2 nanowires.[312-314] Potassium titanate nanowires electrode showed an higher initial discharge capacity of around 305 $mA\cdot h\cdot g^{-1}$ at a current density of 0.05 $mA\cdot cm^{-2}$.[315] Li's group first reported a facile hydrothermal route for preparing TiO_2(B) nanowires with ultrahigh surface area.[316] The surface area can be adjusted by the hydrothermal temperature, and a maximum surface area can be up to 210 $m^2\cdot g^{-1}$. It can be seen from Figure 26b that the initial discharge capacities of TiO_2(B) prepared at 120, 150 and 180 °C were 364, 388 and 379 $mA\cdot h\cdot g^{-1}$, respectively. The obtained TiO_2(B) nanowires proved to be a good anode material for lithium-ion batteries, especially on the fast charging and discharging performance. Besides, Zhang et al. prepared N-doped TiO_2(B) nanowires by solvothermal method. It exhibited a remarkably enhanced electrochemical performance compared to pure TiO_2(B) and show a discharge capacity of 153 $mA\cdot h\cdot g^{-1}$ at the 20 C rate with a capacity retention of 76% after 1000 cycles. In addition, they can deliver a discharge capacity of 100 $mA\cdot h\cdot g^{-1}$ at an ultra-high rate of 100 C, indicating their great potential in high power lithium ion batteries.[317] Except TiO_2(B) nanowires, TiO_2 nanotubes are also widely used as the anode materials of lithium-ion batteries. Li et al. prepared hydrogen titanate nanotubes by hydrothermal in 2005 and it exhibited an initial discharge capacity of 282.2 $mA\cdot h\cdot g^{-1}$ at a current density of 0.24 $A\cdot g^{-1}$.[318] However, the short and irregular TiO_2 nanotubes showed low cycling ability and low discharge capacity. Recently, Chen et al. made a breakthrough on this problem.[85] They synthesized ultralong and uniform TiO_2 nanotubes via a novel stirring hydrothermal technique. The assembled cells exhibit high capacity for the first cycle with the discharge and charge capacities around 368 and 279 $mA\cdot h\cdot g^{-1}$ respectively at a current density of C/4. The electrode demonstrates excellent discharge capacities and cycling life due to high conductivity of the long nanotubes and the high aspect ratio. In particular, a capacity of 114 $mA\cdot h\cdot g^{-1}$ can be achieved after 10000 cycles at rate of 25 C, maintaining 100% efficiency (Figure 26c). In addition, this strategy to synthesize elongated nanostructures can be extended to other systems, opening up new opportunities for manufacturing advanced materials for high-performance energy storage devices.

Compared to other typical layered inorganic material (MoS_2, MoO_3, MnO_2, SnO_2 etc.), TiO_2 possesses a low Li-ion diffusivity and electronic conductivity, leading to a relatively low discharge capacity. Therefore, it is necessary to couple TiO_2 with other materials to facilitate the transport of Li ions and electrons. Xu's group successfully prepared MoS_2 nanosheet@TiO_2 nanotube hybrid nanostructures prepared by a facile two-step method (Figure 27a-c).[319] First, porous TiO_2 nanotubes were prefabricated by sol-gel method. And then MoS_2 nanoclusters that consist of ultrathin nanosheets were assembled on the surface of TiO_2 nanotubes through a solvothermal process. The composites show an initial discharge capacity of 931 $mA\cdot h\cdot g^{-1}$ at 100 $mA\cdot g^{-1}$ and remained high capacity after 50 cycles. That is attributed to the unique structure for large surface area and facilitate the transfer of Li ions. Besides, the MoS_2@TiO_2 nanobelt and MoS_2@TiO_2 nanosheet hybrid structures both exhibited a reversible capacity over 700 $mA\cdot h\cdot g^{-1}$ at 100 $mA\cdot g^{-1}$ after 100 cycles with highly stable capacity retention.[320, 321] What's more, a novel synergistic TiO_2/MoO_3 core-shell nanowire array anode has been fabricated via a facile hydrothermal method followed by a subsequent controllable electrodeposition process (Figure 27d-f).[322] Combined with the unique electrochemical properties of nanostructure arrays, the optimized TiO_2/MoO_3 hybrid anode simultaneously exhibits high gravimetric capacity (ca. 670 $mA\cdot h\cdot g^{-1}$; approaching the hybrid's theoretical value), excellent cyclability (> 200 cycles) and good rate capability (up to 2000 $mA\cdot g^{-1}$). In addition, Liao's group synthesized the unique TiO_2-C/MnO_2 core-double-shell nanowires for the first time using as anode materials for lithium ion batteries. Combining both advantages from TiO_2 such as excellent cycle stability, MnO_2 with high capacity (1230 $mA\cdot h\cdot g^{-1}$) and carbon with high conductivity, the TiO_2-C/MnO_2 core-double-shell nanowire electrodes showed a high charge/discharge capacity and excellent rate performance of 332, 298, 235, 186, and 130 $mA\cdot h\cdot g^{-1}$ at 2, 5, 10, 20, and 30 C. Specifically, it also exhibited enhanced electrochemical cycling and rate properties compared to that of the TiO_2 and TiO_2-C nanowires.[323] In general, carbon are widely used to modify 1D TiO_2 nanofibers to improve the capacity and cycle life of LIBs.[324, 325] These results show 1D TiO_2 nanostructures are ideal and promising materials in replacing the commercial carbon electrodes for lithium-ion batteries to offer excellent rate capacity and ultralong cycle life with enhanced safety.

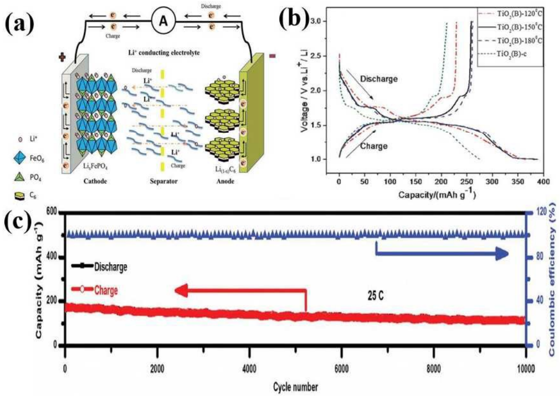

Figure 26. Schematic on the operating principle of traditional rechargeable LIBs (a). Variation of potential (versus a 1 M Li^+/Li electrode) with charge passed for TiO_2(B) nanowires prepared at different hydrothermal temperatures at 10 $mA\cdot g^{-1}$ (b). Long-term cycling performance of TiO_2 nanotubes at a high current density of 25 C (c). Reproduced from ref. 304. Copyright 2014 Royal Society of Chemistry (a). Reproduced from ref. 316. Copyright 2011 Royal Society of Chemistry (b). Reproduced from ref. 85. Copyright 2014 Wiley (c).

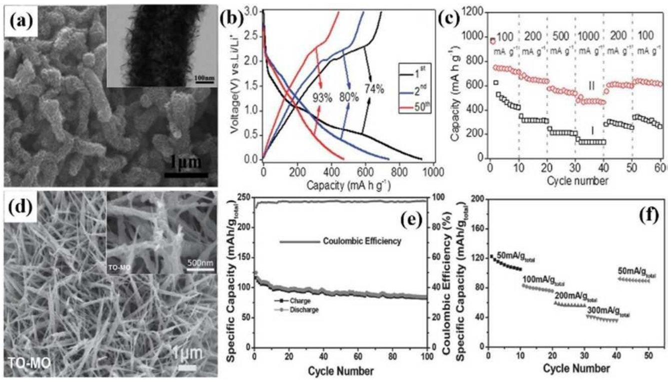

Figure 27. SEM (a) and TEM image (Inset (a)) of MoS_2@TiO_2 hybrids. Charge-discharge voltage profiles at a current density of 100 $mA\cdot g^{-1}$ of MoS_2@TiO_2 hybrid nanostructures (c). Cycling performance of MoS_2 flakes (I) and MoS_2@TiO_2 hybrid nanostructures (II) at different current densities indicated (c). SEM images of TiO_2/MoO_3 core-shell nanowire arrays (d). Cycling performance and coulombic efficiency variation of TiO_2/MoO_3 at $mA\cdot g^{-1}$ (e). Cycling response at progressively increased current densities (f). Reproduced from ref. 319. Copyright 2014 Royal Society of Chemistry (a-c). Reproduced from ref. 322. Copyright 2015 Wiley (d-f).

4.5 Supercapacitors

In response to the changing global landscape, energy has become a primary focus for major corporations and scientific communities all over the world. There has been increasing attention on developing efficient energy storage devices. In recent years, supercapacitors have attracted much interests for use in energy storage due to high power density, fast rates of charge/discharge, reliable cycling life, and safe operation.[326-330] As the electrode material of supercapacitor, the charge storage ability of 1D TiO_2 nanotubes and nanorods (< 1000 $\mu F \cdot cm^{-2}$) is too low due to their low conductivity.[331, 332] Therefore, assembling 1D TiO_2 nanostructures with metal oxides (RuO_2, MnO_2, NiO etc.),[333-335] conducting polymers (PANI) [336] or carbon materials [337] is an efficient approach to obtaining a low-cost, high performance supercapacitors. Li's group deposited hierarchical mesoporous manganese oxide (MnO_x) nanoflakes on nitrided TiO_2 nanorod arrays (NTNA) grown on carbon fiber paper (CFP) by hydrothermal synthesis and electrodeposition.[338] The MnO_x/NTNA/CFP electrode showed high areal capacitance of 327 $mF \cdot cm^{-2}$ at a current density of 0.25 $mA \cdot cm^{-2}$ and good cycling stability with 96% retention after 5000 cycles, which can be attributed to the nitrided TiO_2 nanorod arrays with higher conductivity offering low electrochemical impedance and fast ion/electron transfer (Figure 28a-c). Besides, Shao et al. synthesized polyaniline nanowire/TiO_2 nanotube array electrode for supercapacitors by electro-polymerization.[339] The specific capacitance of these electrodes is around 897.35 $F \cdot g^{-1}$ at a current density of 0.21 $A \cdot g^{-1}$ in 0.05 M H_2SO_4. The modified electrodes also show high cycling stability and maintain 86.2% of the initial capacity after 1500 cycles. Peng's group reported that dye-sensitized solar cell and electrochemical capacitor, coaxially integrated into a novel "energy fiber", can simultaneously realize photoelectric conversion and energy storage (Figure 28d-f).[340] A Ti wire substrate modified with perpendicularly aligned TiO_2 nanotubes on the surface and horizontally aligned multi-walled carbon nanotube sheet serve as two electrodes in the integrated "energy fiber" device. The capacitance was determined by the thickness of carbon nanotubes. A maximal photoelectric conversion efficiency was achieved at 2.73%, while the energy storage efficiency reached 75.7% with specific capacitances up to 3.32 $mF \cdot cm^{-2}$ and power densities up to 0.27 $mW \cdot cm^{-2}$ at a current of 50 μA by using PVA/H_3PO_4 gel electrolyte. The "energy fiber" is flexible and stable, and provides useful experience for various portable electronic devices that require lightweight and weaveable materials. Among the carbon family, graphene are widely used to couple 1D TiO_2 nanostructures as an electrode material for use in electrochemical supercapacitors. It exhibited improved specific capacitance and high cycling stability.[341] As a new category of supercapacitor electrodes, more efforts are underway to further improve the specific capacitance and performance of 1D TiO_2 nanostructured materials.

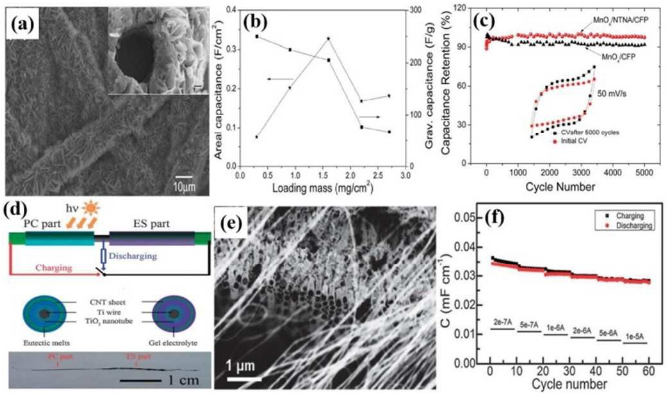

Figure 28. SEM image of MnO_x/NTNA/CFP (a). Plots of gravimetric and areal capacitances versus mass loadings at 0.25 $mA \cdot cm^{-2}$ for MnO_x/NTNA/CFP (b). Cycling performance of the MnO_x/NTNA/CFP and MnO_x/CFP electrodes at 1 $mA \cdot cm^{-2}$ in 1 M Na_2SO_4 for up to 5000 cycles (c). Schematic illustration of the structure of the coaxially integrated dye-sensitized solar cell and electrochemical capacitor into an "energy fiber" (d). SEM images of carbon nanotubes sheet wrapped on the TiO_2 nanotubes (e). Cyclic performance at the increasing electric current (f). Reproduced from ref. 338. Copyright 2015 Wiley (a-c). Reproduced from ref. 340. Copyright 2014 Royal Society of Chemistry (d-f).

5. Conclusions

Up to now, a large number of fundamental studies on synthesis, modification and applications are extensively carried out by many researchers for 1D TiO_2 nanostructured materials. In this review, we present the state-of-the-art development on the fabrication, modification and applications of 1D TiO_2-based materials with well-controlled size and morphology. Guided by the basic formation principles of bulk materials by solid-state reaction, 1D TiO_2 nanostructures can be obtained via hydrothermal method, electrochemical anodization method, vapor deposition method, sol-gel method, template-assisted method and the electrospinning method. Among them, hydrothermal route is most popular for the synthesis of 1D TiO_2 materials due to the easy operation and rational control of the nanostructures. Both enlargement of photocatalytically active area and modification with metal, nonmetal and semiconductors have been employed to improve the performances of 1D TiO_2 nanomaterials. Owing to a high aspect ratio, large specific surface area, excellent electronic or ionic charge transfer property, 1D TiO_2 nanostructured materials are widely used in various applications such as photocatalytic degradation of pollutants, water splitting, solar cells, supercapacitors and lithium batteries.

However, extensive challenges on the functionalities and performances of 1D TiO_2 nanostructures remain. As a wide band gap material, TiO_2 has a low utilization of the full solar energy spectrum, limiting its photocatalystic energy efficiency. Doping and coupling with other nanomaterials have shown good promise, but the cost of production increase. We expect new materials, having the nice attributes of TiO_2 (low cost, stable, non-toxic, easy to prepare into various nanostructures, etc.) with improved light harvesting properties will be discovered / engineered in the future. Meanwhile, it is vital to improve the photoelectrical conversion efficiency for solar cells and lithium batteries through improvement of the transport properties of the 1D TiO_2 nanostructures. With the development of economy and technology, more and more effort will be put into overcoming these drawbacks and endowing TiO_2-based materials with much improved functionalities under reasonable processing cost. In particular, commercialization of these 1D TiO_2-based materials for efficient photocatalysts and photovoltaic materials will be realized in the future.

Acknowledgements

The authors thank the National Natural Science Foundation of China (21501127; 51502185; 51373110), Natural Science Foundation of Jiangsu Province of China (BK20130313; BK20140400), Priority Academic Program Development of Jiangsu Higher Education Institutions (PAPD), Deanship of Scientific Research at King Saud University (PRG-1436-03), and Project for Jiangsu Scientific and Technological Innovation Team (2013) for financial support of this work.

Notes and references

[a]National Engineering Laboratory for Modern Silk, College of Textile and Clothing Engineering, Soochow University, Suzhou 215123, China.

[b]Research Center of Cooperative Innovation for Functional Organic / Polymer Material Micro/Nanofabrication, Soochow University, Suzhou, Suzhou 215123, China.

[c]School of Materials Science and Engineering, Nanyang Technological University, 50 Nanyang Avenue, Singapore 639798, Singapore.

[d]Department of Chemistry, College of Science, King Saud University, Riyadh 11451, Saudi Arabia.

Corresponding author email: yklai@suda.edu.cn

Electronic Supplementary Information (ESI) available: [details of any supplementary information available should be included here]. See DOI: 10.1039/b000000x/

1. E. G. Snyder, T. H. Watkins, P. A. Solomon, E. D. Thoma, R. W. Williams, G. S. W. Hagler, D. Shelow, D. A. Hindin, V. J. Kilaru and P. W. Preuss, *Environ. Sci. Technol.*, 2013, **47**, 11369-11377.
2. J. S. Kim, H. S. Han, S. Shin, G. S. Han, H. S. Jung, K. S. Hong and J. H. Noh, *Inter. J. Hydrogen Energy*, 2014, **39**, 17473-17480.
3. G. C. Xie, K. Zhang, B. D. Guo, Q. Liu, L. Fang and J. R. Gong, *Adv. Mater.*, 2013, **25**, 3820-3839.
4. J. Ran, J. Zhang, J. Yu, M. Jaroniec and S. Z. Qiao, *Chem. Soc. Rev.*, 2014, **43**, 7787-7812.
5. P. D. Tran, L. H. Wong, J. Barber and J. S. C. Loo, *Energy Environ. Sci.*, 2012, **5**, 5902-5918.
6. S. Hu, B. Chi, J. Pu and L. Jian, *J.Mater. Chem. A*, 2014, **2**, 19260-19267.
7. C. Liu, F. Li, L. P. Ma and H. M. Cheng, *Advanced Materials*, 2010, **22**, E26-E28.
8. I. Y. Jeon, M. J. Ju, J. Xu, H. J. Choi, J. M. Seo, M. J. Kim, I. T. Choi, H. M. Kim, J. C. Kim, J. J. Lee, H. K. Liu, H. K. Kim, S. Dou, L. Dai and J. B. Baek, *Adv. Funct. Mater.*, 2015, **25**, 1170-1179.
9. S. Li, Y. Luo, W. Lv, W. Yu, S. Wu, P. Hou, Q. Yang, Q. Meng, C. Liu and H. M. Cheng, *Adv. Energy Mater.*, 2011, **1**, 486-490.
10. A. Fujishima and K. Honda, *Nature*, 1972, **238**, 37-39.
11. H. Y. Liu, J. B. Joo, M. Dahl, L. S. Fu, Z. Z. Zeng and Y. D. Yin, *Energ. Environ. Sci.*, 2015, **8**, 286-296.
12. H. F. Zhuang, C. J. Lin, Y. K. Lai, L. Sun and J. Li, *Environ. Sci. Technol.*, 2007, **41**, 4735-4740.
13. W. J. Ong, L. L. Tan, S. P. Chai, S. T. Yong and A. R. Mohamed, *ChemSusChem*, 2014, **7**, 690-719.
14. L. L. Tan, W. J. Ong, S. P. Chai, S. T. Yong and A. R. Mohamed, *Nano Research*, 2014, **7**, 1528-1547.
15. B. Seger, T. Pedersen, A. B. Laursen, P. C. K. Vesborg, O. Hansen and I. Chorkendorff, *J. Am. Chem. Soc.*, 2013, **135**, 1057-1064.
16. Q. Kang, J. Y. Cao, Y. J. Zhang, L. Q. Liu, H. Xu and J. H. Ye, *J. Mater. Chem. A*, 2013, **1**, 5766-5774.
17. Y. J. Ji, M. D. Zhang, J. H. Cui, K. C. Lin, H. G. Zheng, J. J. Zhu and A. C. S. Samia, *Nano Energy*, 2012, **1**, 796-804.
18. P. Roy, D. Kim, K. Lee, E. Spiecker and P. Schmuki, *Nanoscale*, 2010, **2**, 45-59.
19. H. Li, Z. H. Chen, C. K. Tsang, Z. Li, X. Ran, C. Lee, B. Nie, L. X. Zheng, T. F. Hung, J. Lu, B. C. Pan and Y. Y. Li, *J. Mater. Chem. A*, 2014, **2**, 229-236.
20. B. Chen, J. B. Hou and K. Lu, *Langmuir*, 2013, **29**, 5911-5919.
21. Y. K. Lai, L. X. Lin, F. Pan, J. Y. Huang, R. Song, Y. X. Huang, C. J. Lin, H. Fuchs and L. F. Chi, *Small*, 2013, **9**, 2945-2953.
22. H. Q. Li, Y. K. Lai, J. Y. Huang, Y. X. Tang, L. Yang, Z. Chen, K. Q. Zhang, X. C. Wang and L. P. Tan, *J. Mater. Chem. B*, 2015, **3**, 342-347.
23. J. S. Chen, Y. L. Tan, C. M. Li, Y. L. Cheah, D. Y. Luan, S. Madhavi, F. Y. C. Boey, L. A. Archer and X. W. Lou, *J. Am. Chem. Soc.*, 2010, **132**, 6124-6130.
24. K. X. Wang, M. D. Wei, M. A. Morris, H. S. Zhou and J. D. Holmes, *Adv. Mater.*, 2007, **19**, 3016-3020.
25. B. Liu, K. Nakata, M. Sakai, H. Saito, T. Ochiai, T. Murakami, K. Takagi and A. Fujishima, *Catal. Sci. Technol.*, 2012, **2**, 1933-1939.
26. P. Hartmann, D.-K. Lee, B. M. Smarsly and J. Janek, *ACS Nano*, 2010, **4**, 3147-3154.
27. G. S. Han, S. Lee, J. H. Noh, H. S. Chung, J. H. Park, B. S. Swain, J. H. Im, N. G. Park and H. S. Jung, *Nanoscale*, 2014, **6**, 6127-6132.
28. Y. Tang, Y. Lai, D. Goog, K. H. Goh, T. T. Lim, Z. Dong and Z. Chen, *Chem. Eur. J.*, 2010, **16**, 7704-7708.
29. Z. Wu, Y. Wang, L. Sun, Y. Mao, M. Wang and C. Lin, *J. Mater. Chem. A*, 2014, **2**, 8223-8229.
30. M. Z. Ge, C. Y. Cao, S. H. Li, S. N. Zhang, S. Deng, J. Y. Huang, Q. S. Li, K. Q. Zhang, S. S. Al-Deyab and Y. K. Lai, *Nanoscale*, 2015, **7**, 11552-11560.
31. N. Kijima, M. Kuwabara, J. Akimoto, T. Kumagai, K. Igarashi and T. Shimizu, *J. Power Sources*, 2011, **196**, 7006-7010.
32. C. S. Lee, J. K. Kim, J. Y. Lim and J. H. Kim, *ACS Appl. Mater. Interfaces*, 2014, **6**, 20842-20850.
33. H. Yao, W. Fu, H. Yang, J. Ma, M. Sun, Y. Chen, W. Zhang, D. Wu, P. Lv and M. Li, *Electrochim. Acta*, 2014, **125**, 258-265.
34. W. J. Zhou, Z. Y. Yin, Y. P. Du, X. Huang, Z. Y. Zeng, Z. X. Fan, H. Liu, J. Y. Wang and H. Zhang, *Small*, 2013, **9**, 140-147.
35. S. J. Kim, Y. K. Cho, J. Seok, N. S. Lee, B. Son, J. W. Lee, J. M. Baik, C. Lee, Y. Lee and M. H. Kim, *ACS Appl. Mater. Interfaces*, 2015, **7**, 15321-15330.
36. J. Y. Huang, Y. K. Lai, F. Pan, L. Yang, H. Wang, K. Q. Zhang, H. Fuchs and L. F. Chi, *Small*, 2014, **10**, 4865-4873.
37. Y. K. Lai, J. Y. Huang, Z. Q. Cui, M. Z. Ge, K. Q. Zhang, Z. Chen and L. F. Chi, *Small*, 2016, **11**, DOI: 10.1002/smll.201501837.
38. A. N. Banerjee, *Nanotechnol. Sci. Appl.*, 2011, **4**, 35-65.
39. Y. K. Lai, L. N. Wang, D. W. Liu, Z. Chen and C. J. Lin, *J. Nanomater.*, 2015, **2015**, 250632.
40. W. J. Zhou, H. Liu, R. I. Boughton, G. J. Du, J. J. Lin, J. Y. Wang and D. Liu, *J. Mater. Chem.*, 2010, **20**, 5993-6008.
41. J. Zhang, F. X. Xiao, G. Xiao and B. Liu, *Nanoscale*, 2014, **6**, 11293-11302.
42. K. Pan, Y. Z. Dong, C. G. Tian, W. Zhou, G. H. Tian, B. F. Zhao and H. G. Fu, *Electrochim. Acta*, 2009, **54**, 7350-7356.
43. M. A. Hossain, J. Park, J. Y. Ahn, C. Park, Y. Kim, S. H. Kim and D. Lee, *Electrochim. Acta*, 2015, **173**, 665-671.
44. Z. Gyori, Z. Konya and A. Kukovecz, *Appl. Catal. B-Environ.*, 2015, **179**, 583-588.
45. S. H. Ahn, W. S. Chi, J. T. Park, J. K. Koh, D. K. Roh and J. H. Kim, *Adv. Mater.*, 2012, **24**, 519-522.
46. M. Z. Ge, C. Y. Cao, J. Y. Huang, S. H. Li, S. N. Zhang, S. Deng, Q. S. Li, K. Q. Zhang and Y. K. Lai, *Nanotechnology Rev.*, 2016, **5**, DOI: 10.1515/ntrev-2015-0049.
47. Y. Y. Zhang, Z. L. Jiang, J. Y. Huang, L. Y. Lim, W. L. Li, J. Y. Deng, D. Gong, Y. X. Tang, Y. K. Lai and Z. Chen, *RSC Adv.*, 2015, **5**, 79479-79510.
48. J. Muscat, V. Swamy and N. M. Harrison, *Phys. Rev. B*, 2002, **65**, 224112.
49. M. Altomare, M. V. Dozzi, G. L. Chiarello, A. Di Paola, L. Palmisano and E. Selli, *Catal. Today*, 2015, **252**, 184-189.
50. Z. W. Yang, B. Wang, H. Cui, H. An, Y. Pan and J. P. Zhai, *J. Phys. Chem. C*, 2015, **119**, 16905-16912.
51. M. Alsawat, T. Altalhi, J. G. Shapter and D. Losic, *Catal. Sci. Technol.*, 2014, **4**, 2091-2098.
52. Y. Mi and Y. X. Weng, *Sci. Rep.*, 2015, **5**, 11482.
53. Q. L. Tay, X. F. Liu, Y. X. Tang, Z. L. Jiang, T. C. Sum and Z. Chen, *J. Phys. Chem. C*, 2013, **117**, 14973-14982.
54. J. Dai, J. Yang, X. H. Wang, L. Zhang and Y. J. Li, *Appl. Surf. Sci.*, 2015, **349**, 343-352.
55. L. H. Qi, C. Y. Li and Y. J. Chen, *Chem. Phys. Lett.*, 2012, **539**, 128-132.
56. A. G. Dylla, P. Xiao, G. Henkelman and K. J. Stevenson, *J. Physical Chem. Lett.*, 2012, **3**, 2015-2019.

57. D. J. Yang, H. W. Liu, Z. F. Zheng, Y. Yuan, J. C. Zhao, E. R. Waclawik, X. B. Ke and H. Y. Zhu, *J. Am. Chem. Soc.*, 2009, **131**, 17885-17893.

58. Z. F. Zheng, H. W. Liu, J. P. Ye, J. C. Zhao, E. R. Waclawik and H. Y. Zhu, *J. Mol. Catal. A-Chem.*, 2010, **316**, 75-82.

59. J. J. Yang, Z. S. Jin, X. D. Wang, W. Li, J. W. Zhang, S. L. Zhang, X. Y. Guo and Z. J. Zhang, *Dalton Trans.*, 2003, 3898-3901.

60. G. H. Du, Q. Chen, R. C. Che, Z. Y. Yuan and L. M. Peng, *Appl. Phys. Lett.*, 2001, **79**, 3702-3704.

61. D. Li, Z. P. Xing, X. J. Yu and X. W. Cheng, *Electrochim. Acta*, 2015, **170**, 182-190.

62. X. J. Hu, Y. K. Shi, Y. J. Zhang, B. L. Zhu, S. M. Zhang and W. P. Huang, *Catal. Commun.*, 2015, **59**, 45-49.

63. L. L. Lai and J. M. Wu, *J. Mater. Chem. A*, 2015, **3**, 15863-15868.

64. Z. H. Zhao, J. Tian, D. Z. Wang, X. L. Kang, Y. H. Sang, H. Liu, J. Y. Wang, S. W. Chen, R. I. Boughton and H. D. Jiang, *J. Mater. Chem.*, 2012, **22**, 23395-23403.

65. Y. S. Luo, D. Z. Kong, J. S. Luo, S. Chen, D. Y. Zhang, K. W. Qiu, X. Y. Qi, H. Zhang, C. M. Li and T. Yu, *RSC Adv.*, 2013, **3**, 14413-14422.

66. T. Kasuga, M. Hiramatsu, A. Hoson, T. Sekino and K. Niihara, *Langmuir*, 1998, **14**, 3160-3163.

67. T. Kasuga, M. Hiramatsu, A. Hoson, T. Sekino and K. Niihara, *Adv. Mater.*, 1999, **11**, 1307-1311.

68. G. Armstrong, A. R. Armstrong, J. Canales and P. G. Bruce, *Chem. Commun.*, 2005, 2454-2456.

69. D. V. Bavykin, V. N. Parmon, A. A. Lapkin and F. C. Walsh, *J. Mater. Chem.*, 2004, **14**, 3370-3377.

70. R. L. Dong, S. J. Jiang, Z. Li, Z. Y. Chen, H. P. Zhang and C. C. Jin, *Mater. Lett.*, 2015, **152**, 151-154.

70. B. Liu and E. S. Aydil, *J. Am. Chem. Soc.*, 2009, **131**, 3985-3990.

72. Y. B. Xie, C. Xia, H. X. Du and W. Wang, *J. Power Sources*, 2015, **286**, 561-570.

73. J. Y. Liao, B. X. Lei, H. Y. Chen, D. B. Kuang and C. Y. Su, *Energy Environ. Sci.*, 2012, **5**, 5750-5757.

74. D. Sarkar and K. K. Chattopadhyay, *ACS Appl. Mater. Interfaces*, 2014, **6**, 10044-10059.

75. M. C. Li, Y. J. Jiang, R. Q. Ding, D. D. Song, H. Yu and Z. Chen, *J Electron. Mater.*, 2013, **42**, 1290-1296.

76. F. R. Wang, G. Q. Zhang, Z. Zhao, H. Q. Tan, W. X. Yu, X. M. Zhang and Z. C. Sun, *RSC Adv.*, 2015, **5**, 9861-9864.

77. S. L. Feng, J. Y. Yang, H. Zhu, M. Liu, J. S. Zhang, J. Wu and J. Y. Wan, *J. Am. Ceram. Soc.*, 2011, **94**, 310-315.

78. J. Tian, Z. H. Zhao, A. Kumar, R. I. Boughton and H. Liu, *Chem. Soc. Rev.*, 2014, **43**, 6920-6937.

79. S. H. Lim, J. Z. Luo, Z. Y. Zhong, W. Ji and J. Y. Lin, *Inorg. Chem.*, 2005, **44**, 4124-4126.

80. A. Nakahira, T. Kubo and C. Numako, *Inorg. Chem.*, 2010, **49**, 5845-5852.

81. D. L. Morgan, H. Y. Zhu, R. L. Frost and E. R. Waclawik, *Chem. Mater.*, 2008, **20**, 3800-3802.

82. X. S. Peng and A. C. Chen, *Adv. Funct. Mater.*, 2006, **16**, 1355-1362.

83. S. I. Tanaka, N. Hirose and T. Tanaki, *J. Electrochem. Soc.*, 2005, **152**, C789-C794.

84. Y. X. Tang, Y. Y. Zhang, J. Y. Deng, D. P. Qi, W. R. Leow, J. Q. Wei, S. Y. Yin, Z. L. Dong, R. Yazami, Z. Chen and X. D. Chen, *Angew. Chem. Int. Ed.*, 2014, **53**, 13488-13492.

85. Y. X. Tang, Y. Y. Zhang, J. Y. Deng, J. Q. Wei, T. L. Hon, B. K. Chandran, Z. L. Dong, Z. Chen and X. D. Chen, *Adv. Mater.*, 2014, **26**, 6111-6118.

86. Q. Y. Jia, W. X. Que and J. Zhang, *Phys. Status Solidi A*, 2011, **208**, 2313-2316.

87. C. T. Nam, J. L. Falconer, L. M. Du and W. D. Yang, *Mater. Res. Bull.*, 2014, **51**, 49-55.

88. P. F. Wang, Y. H. Ao, C. Wang, J. Hou and J. Qian, *Mater. Lett.*, 2013, **101**, 41-43.

89. N. T. Q. Hoa and D. N. Huyen, *J. Mater. Sci.*, 2013, **24**, 793-798.

90. Y. J. Chen, G. H. Tian, Z. Y. Ren, C. G. Tian, K. Pan. W. Zhou and H. G. Fu, *Eur. J. Inorg. Chem.*, 2011, **5**, 754-760.

91. Q. Wang, Z. H. Wen and J. H. Li, *Inorg. Chem.*, 2006, **45**, 6944-6949.

92. Z. L. He, W. X. Que, J. Chen, X. T. Yin, Y. C. He and J. B. Ren, *ACS Appl. Mater. Interfaces*, 2012, **4**, 6816-6826.

93. J. Y. Zhao, J. X. Yao, Y. Z. Zhang, M. N. Guli and L. Xiao, *J. Power Sources*, 2014, **255**, 16-23.

94. M. Assefpourdezfuly, C. Vlachos and E. H. Andrews, *J. Mater. Sci.*, 1984, **19**, 3626-3639.

95. V. Zwilling, E. Darque-Ceretti, A. Boutry-Forveille, D. David, M. Y. Perrin and M. Aucouturier, *Surf. Interface Anal.*, 1999, **27**, 629-637.

96. J. M. Macak, K. Sirotna and P. Schmuki, *Electrochim. Acta*, 2005, **50**, 3679-3684.

97. M. Paulose, H. E. Prakasam, O. K. Varghese, L. Peng, K. C. Popat, G. K. Mor, T. A. Desai and C. A. Grimes, *J. Phys. Chem. C*, 2007, **111**, 14992-14997.

98. R. Hahn, J. M. Macak and P. Schmuki, *Electrochem. Commun.*, 2007, **9**, 947-952.

99. M. Z. Ge, S. H. Li, J. Y. Huang, K. Q. Zhang, S. S. Al-Deyab and Y. K. Lai, *J. Mater. Chem. A*, 2015, **3**, 3491-3499.

100. M. D. Ye, J. J. Gong, Y. K. Lai, C. J. Lin and Z. Q. Lin, *J. Am. Chem. Soc.*, 2012, **134**, 15720-15723.

101. J. Du, X. Gu, H. Z. Guo, J. Liu, Q. Wu and J. G. Zou, *J. Cryst. Growth*, 2015, **427**, 54-59.

102. C. A. Chen, Y. M. Chen, A. Korotcov, Y. S. Huang, D. S. Tsai and K. K. Tiong, *Nanotechnology*, 2008, **19**, 075611.

103. N. T. Q. Hoa and E. T. Kim, *Electrochem. Solid-State Lett.*, 2008, **11**, K1-K3.

104. M. S. Sander, M. J. Cote, W. Gu, B. M. Kile and C. P. Tripp, *Adv. Mater.*, 2004, **16**, 2052-2057.

105. J. Joo, S. G. Kwon, T. Yu, M. Cho, J. Lee, J. Yoon and T. Hyeon, *J. Phys. Chem. B*, 2005, **109**, 15297-15302.

106. J. J. Qiu, W. D. Yu, X. D. Gao and X. M. Li, *Nanotechnology*, 2006, **17**, 4695-4698.

107. A. S. Attar, M. S. Ghamsari, F. Hajiesmaeilbaigi, S. Mirdamadi, K. Katagiri and K. Koumoto, *Mater. Chem. Phys.*, 2009, **113**, 856-860.

108. Y. Lin, G. S. Wu, X. Y. Yuan, T. Xie and L. D. Zhang, *J. Phys.: Condens. Matter*, 2003, **15**, 2917-2922.

109. D. Li and Y. N. Xia, *Nano Lett.*, 2003, **3**, 555-560.

110. Y. Yang, H. Y. Wang, Q. W. Zhou, M. Q. Kong, H. T. Ye and G. Yang, *Nanoscale*, 2013, **5**, 10267-10274.

111. F. L. Zhang, Z. Q. Cheng, L. J. Kang, L. Y. Cui, W. Liu, X. J. Xu, G. H. Hou and H. J. Yang, *RSC Adv.*, 2015, **5**, 32088-32091.

112. L. L. Zhu, M. H. Hong and G. W. Ho, *Nano Energy*, 2015, **11**, 28-37.

113. A. G. El-Deen, J. H. Choi, K. A. Khalil, A. A. Almajid and N. A. M. Barakat, *RSC Adv.*, 2014, **4**, 64634-64642.

114. P. F. Du, L. X. Song, J. Xiong, N. Li, Z. Q. Xi, L. C. Wang, D. L. Jin, S. Y. Guo and Y. F. Yuan, *Electrochim. Acta*, 2012, **78**, 392-397.

115. Y. Hou, X. Y. Li, Q. D. Zhao, X. Quan and G. H. Chen, *J. Mater. Chem.*, 2011, **21**, 18067-18076.

116. Y. C. Yang, X. B. Ji, M. J. Jing, H. S. Hou, Y. R. Zhu, L. B. Fang, X. M. Yang, Q. Y. Chen and C. E. Banks, *J. Mater. Chem. A*, 2015, **3**, 5648-5655.

117. H. Y. Wang, G. M. Wang, Y. C. Ling, M. Lepert, C. C. Wang, J. Z. Zhang and Y. Li, *Nanoscale*, 2012, **4**, 1463-1466.

118. X. Meng, D. W. Shin, S. M. Yu, J. H. Jung, H. I. Kim, H. M. Lee, Y. H. Han, V. Bhoraskar and J. B. Yoo, *Crystengcomm*, 2011, **13**, 3021-3029.

119. M. Y. Wang, D. J. Zheng, M. D. Ye, C. C. Zhang, B. B. Xu, C. J. Lin, L. Sun and Z. Q. Lin, *Small*, 2015, **11**, 1436-1442.

120. W. J. Zhou, G. J. Du, P. G. Hu, G. H. Li, D. Z. Wang, H. Liu, J. Y. Wang, R. I. Boughton, D. Liu and H. D. Jiang, *J. Mater. Chem.*, 2011, **21**, 7937-7945.

121. M. Lazzeri, A. Vittadini and A. Selloni, *Phys. Rev. B*, 2002, **65**, 119901.

122. X. Q. Gong and A. Selloni, *J. Phys. Chem. B*, 2005, **109**, 19560-19562.

123. Z. H. Zhang, X. H. Zhong, S. H. Liu, D. F. Li and M. Y. Han, *Angew. Chem. Int. Ed.*, 2005, **44**, 3466-3470.

124. H. G. Yang, C. H. Sun, S. Z. Qiao, J. Zou, G. Liu, S. C. Smith, H. M. Cheng and G. Q. Lu, *Nature*, 2008, **453**, 638-U634.

125. Y. H. Fan, C. H. Ma, B. Y. Liu, H. Y. Chen, L. H. Dong and Y. S. Yin, *Mater. Sci. Semicon. Proc.*, 2014, **27**, 47-50.

126. M. C. Wen, P. J. Liu, S. N. Xiao, K. Mori, Y. Kuwahara, H. X. Yamashita, H. Li and D. Q. Zhang, *RSC Adv.*, 2015, **5**, 11029-11035.

127. X. H. Yang, Z. Li, C. Sun, H. G. Yang and C. Li, *Chem. Mater.*, 2011, **23**, 3486-3494.

128. Z. L. Jiang, Y. X. Tang, Q. L. Tay, Y. Y. Zhang, O. I. Malyi, D. P. Wang, J. Y. Deng, Y. K. Lai, H. F. Zhou, X. D. Chen, Z. L. Dong and Z. Chen, *Adv. Energy Mater.*, 2013, **3**, 1368-1380.

129. S. W. Liu, J. Q. Yu and M. Jaroniec, *Chem. Mater.*, 2011, **23**, 4085-4093.

130. C. Z. Wen, J. Z. Zhou, H. B. Jiang, Q. H. Hu, S. Z. Qiao and H. G. Yang, *Chem. Commun.*, 2011, **47**, 4400-4402.

131. J. G. Yu, J. J. Fan and K. L. Lv, *Nanoscale*, 2010, **2**, 2144-2149.

132. R. Asahi, T. Morikawa, T. Ohwaki, K. Aoki and Y. Taga, *Science*, 2001,

293, 269-271.
133. X. Hou, C. W. Wang, W. D. Zhu, X. Q. Wang, Y. Li, J. Wang, J. B. Chen, T. Gan, H. Y. Hu and F. Zhou, *Solid State Sci.*, 2014, **29**, 27-33.
134. F. Wang and D. G. Li, *Mater. Lett.*, 2015, **158**, 119-122.
135. J. Hu, H. S. Li, Q. Wu, Y. Zhao and Q. Z. Jiao, *Chem. Eng. J.*, 2015, **263**, 144-150.
136. S. W. Shin, J. Y. Lee, K. S. Ahn, S. H. Kang and J. H. Kim, *J. Phys. Chem. C*, 2015, **119**, 13375-13383.
137. Y. Komaia, K. Okitsua, R. Nishimuraa, N. Ohtsub, G. Miyamotoc, T. Furuharac, S. Semboshic, Y. Mizukoshid, N. Masahashid, *Catal. Today*, 2011, **164**, 399-403.
138. Z. L. Hua, Z. Y. Dai, X. Bai, Z. F. Ye, H. X. Gu and X. Huang, *J. Hazard. Mater.*, 2015, **293**, 112-121.
139. R. Ramanathan and V. Bansal, *RSC Adv.*, 2015, **5**, 1424-1429.
140. Y. Zhang, M. Creatore, Q. B. Ma, A. El Boukili, L. Gao, M. A. Verheijen, M. W. G. M. Verhoeven and E. J. M. Hensen, *Appl. Surf. Sci.*, 2015, **330**, 476-486.
141. A. Ghicov, J. M. Macak, H. Tsuchiya, J. Kunze, V. Haeublein, S. Kleber and P. Schmuki, *Chem. Phys. Lett.*, 2006, **419**, 426-429.
142. B. Gao, X. X. Li, Y. W. Ma, Y. Cao, Z. Y. Hu, X. M. Zhang, J. J. Fu, K. F. Huo and P. K. Chu, *Thin Solid Films*, 2015, **584**, 61-65.
143. P. S. Saud, B. Pant, A. M. Alam, Z. K. Ghouri, M. Park and H. Y. Kim, *Ceram. Int.*, 2015, **41**, 11953-11959.
144. Z. L. He, W. X. Que, J. Chen, X. T. Yin, Y. C. He and J. B. Ren, *ACS Appl. Mater. Interfaces*, 2012, **4**, 6815-6825.
145. Q. J. Xiang, J. G. Yu and M. Jaroniec, *Phys. Chem. Chem. Phys.*, 2011, **13**, 4853-4861.
146. J. G. Yu, Q. J. Xiang and M. H. Zhou, *Appl. Catal. B:Environ.*, 2009, **90**, 595-602.
147. J.-N. Nian, S.-A. Chen, C.-C. Tsai and H. Teng, *J. Phys. Chem. B*, 2006, **110**, 25817-25824.
148. S. N. R. Inturi, T. Boningari, M. Suidan and P. G. Smirniotis, *Appl. Catal. B-Environ.*, 2014, **144**, 333-342.
149. Y. F. Su, Z. Wu, Y. N. Wu, J. D. Yu, L. Sun and C. J. Lin, *J. Mater. Chem. A*, 2015, **3**, 8537-8544.
150. Y.-C. Pu, G. Wang, K.-D. Chang, Y. Ling, Y.-K. Lin, B. C. Fitzmorris, C.-M. Liu, X. Lu, Y. Tong, J. Z. Zhang, Y.-J. Hsu and Y. Li, *Nano Lett.*, 2013, **13**, 3817-3823.
151. L. Sun, J. Li, C. L. Wang, S. F. Li, Y. K. Lai, H. B. Chen and C. J. Lin, *J. Hazard. Mater.*, 2009, **171**, 1045-1050.
152. J. G. Yu, L. F. Qi and M. Jaroniec, *J. Phys. Chem. C*, 2010, **114**, 13118-13125.
153. T. T. Jiang, C. C. Jia, L. C. Zhang, S. R. He, Y. H. Sang, H. D. Li, Y. Q. Li, X. H. Xu and H. Liu, *Nanoscale*, 2015, **7**, 209-217.
154. H. Hua, C. G. Hu, Z. H. Zhao, H. Liu, X. Xie and Y. Xi, *Electrochim. Acta*, 2013, **105**, 130-136.
155. W. J. Zhou, G. J. Du, P. G. Hu, Y. Q. Yin, J. H. Li, J. H. Yu, G. C. Wang, J. X. Wang, H. Liu, J. Y. Wang and H. Zhang, *J. Hazard. Mater.*, 2011, **197**, 19-25.
156. J. G. Li, T. T. Zhao, T. K. Chen, Y. B. Liu, C. N. Ong and J. P. Xie, *Nanoscale*, 2015, **7**, 7502-7519.
157. B. X. Chen, W. F. Zhang, X. H. Zhou, X. Huang, X. M. Zhao, H. T. Wang, M. Liu, Y. L. Lu and S. F. Yang, *Nano Energy*, 2013, **2**, 906-915.
158. C. H. Lin, J. H. Chao, W. J. Tsai, M. J. He and T. J. Chiang, *Phys. Chem. Chem. Phys.*, 2014, **16**, 23743-23753.
159. M. Ghaffari, M. B. Cosar, H. I. Yavuz, M. Ozenbas and A. K. Okyay, *Electrochim. Acta*, 2012, **76**, 446-452.
160. S. H. Nam, H.-S. Shim, Y.-S. Kim, M. A. Dar, J. G. Kim and W. B. Kim, *ACS Appl. Mater. Interfaces*, 2010, **2**, 2046-2052.
161. S. Sarker, B. Mukherjee, E. Crone and V. Subramanian, *J. Mater. Chem. A*, 2014, **2**, 4890-4893.
162. Y. Yang and W. Y. Wang, *J. Power Sources*, 2015, **293**, 577-584.
163. P. Pathak, S. Gupta, K. Grosulak, H. Imahori and V. Subramanian, *J. Phys. Chem. C*, 2015, **119**, 7543-7553.
164. Z. B. Shao, W. Zhu, Z. Li, Q. H. Yang and G. Z. Wang, *J. Phys. Chem. C*, 2012, **116**, 2438-2442.
165. D. H. Kim, H. S. Han, I. S. Cho, W. M. Seong, I. J. Park, J. H. Park, S. Shin, G. Do Park, S. Park, S. Lee and K. S. Hong, *Int. J. Hydrogen Energy*, 2015, **40**, 863-869.
166. Y. Xie, G. Ali, S. H. Yoo and S. O. Cho, *ACS Appl. Mater. Interfaces*, 2010, **2**, 2910-2914.
167. Y. Liu, L. Zhao, M. T. Li and L. J. Guo, *Nanoscale*, 2014, **6**, 7397-7404.
168. H.-S. Rao, W.-Q. Wu, Y. Liu, Y.-F. Xu, B.-X. Chen, H.-Y. Chen, D.-B. Kuang and C.-Y. Su, *Nano Energy*, 2014, **8**, 1-8.
169. Z. Y. Zhang, C. L. Shao, X. H. Li, C. H. Wang, M. Y. Zhang and Y. C. Liu, *ACS Appl. Mater. Interfaces*, 2010, **2**, 2915-2923.
170. H. C. He, P. Xiao, M. Zhou, Y. H. Zhang, Q. Lou and X. Z. Dong, *Int. J. Hydrogen Energy*, 2012, **37**, 4967-4973.
171. C. Chen, W. M. Cai, M. C. Long, B. X. Zhou, Y. H. Wu, D. Y. Wu and Y. J. Feng, *ACS Nano*, 2010, **4**, 6425-6432.
172. M. Y. Wang, L. Sun, Z. Q. Lin, J. H. Cai, K. P. Xie and C. J. Lin, *Energy Environ. Sci.*, 2013, **6**, 1211-1220.
173. J. Deng, L. Wang, Z. Lou and T. Zhang, *J. Mater. Chem. A*, 2014, **2**, 9030-9034.
174. M. D. Ye, X. K. Xin, C. J. Lin and Z. Q. Lin, *Nano Lett.*, 2011, **11**, 3214-3220.
175. W. J. Yue, C. W. Liu, Z. L. Qiu and M. T. Wang, *Sol. Energy*, 2015, **113**, 358-368.
176. X. M. Zhang, B. Gao, L. S. Hu, L. M. Li, W. H. Jin, K. F. Huo and P. K. Chu, *Crystengcomm*, 2014, **16**, 10280-10285.
177. Z. Wu, Y. F. Su, J. D. Yu, W. Xiao, L. Sun and C. J. Lin, *Int. J. Hydrogen Energy*, 2015, **40**, 9704-9712.
178. H.-S. Kim, J.-W. Lee, N. Yantara, P. P. Boix, S. A. Kulkarni, S. Mhaisalkar, M. Graetzel and N.-G. Park, *Nano Lett.*, 2013, **13**, 2412-2417.
179. D. Chen, H. Zhang, Y. Liu and J. H. Li, *Energy Environ. Sci.*, 2013, **6**, 1362-1387.
180. Y. Y. Wen, H. M. Ding and Y. K. Shan, *Nanoscale*, 2011, **3**, 4411-4417.
181. Y. B. Liu, J. H. D. Lee, Q. Xia, Y. Ma, Y. Yu, L. Y. L. Yung, J. P. Xie, C. N. Ong, C. D. Vecitis and Z. Zhou, *J. Mater. Chem. A*, 2014, **2**, 16554-16562.
182. S. Gupta and V. Subramaniant, *ACS Appl. Mater. Interfaces*, 2014, **6**, 18597-18608.
183. Q. J. Xiang, J. G. Yu and M. Jaroniec, *Nanoscale*, 2011, **3**, 3670-3678.
184. S. D. Perera, R. G. Mariano, K. Vu, N. Nour, O. Seitz, Y. Chabal and K. J. Balkus, *ACS Catal.*, 2012, **2**, 949-956.
185. X. Pan, Y. Zhao, S. Liu, C. L. Korzeniewski, S. Wang, and Z. Y. Fan, *ACS Appl. Mater. Interfaces*, 2012, **4**, 3944-3950.
186. Y. K. Lai, L. Sun, Y. C. Chen, H. F. Zhuang, C. J. Lin and J. W. Chin, *J. Electrochem. Soc.*, 2006, **153**, D123-D127.
187. S. D. Wang, Q. Ma, H. Liu, K. Wang, L. Z. Ling and K. Q. Zhang, *RSC Adv.*, 2015, **5**, 40521-40530.
188. D. Yang, Y. Y. Sun, Z. W. Tong, Y. Tian, Y. B. Li and Z. Y. Jiang, *J. Phys. Chem. C*, 2015, **119**, 5827-5835.
189. P. Zhang, C. L. Shao, Z. Y. Zhang, M. Y. Zhang, J. B. Mu, Z. C. Guo and Y. C. Liu, *Nanoscale*, 2011, **3**, 2943-2949.
190. J. F. Zhang, Y. Wang, C. P. Yu, X. Shu, L. Jiang, J. W. Cui, Z. Chen, T. Xie and Y. C. Wu, *New J. Chem.*, 2014, **38**, 4975-4984.
191. W. Liu, J. R. Li and X. C. Yin, *Water Res.*, 2014, **53**, 12-25.
192. D. Z. Lu, P. F. Fang, X. Z. Liu, S. B. Zhai, C. H. Li, X. N. Zhao, J. Q. Ding and R. Y. Xiong, *Appl. Catal. B:Environ.*, 2015, **179**, 558-573.
193. M. Y. Wang, J. Ioccozia, L. Sun, C. J. Lin and Z. Q. Lin, *Energy Environ. Sci.*, 2014, **7**, 2182-2202.
194. L. Wu, F. Li, Y. Y. Xu, J. W. Zhang, D. Q. Zhang, G. S. Li and H. X. Li, *Appl. Catal. B:Environ.*, 2015, **164**, 217-224.
195. Y. K. Lai, J. Y. Huang, H. F. Zhuang, V. P. Subramaniam, Y. X. Tang, D. G. Gong, L. Sundar, L. Sun, Z. Chen and C. J. Lin, *J. Hazard. Mater.*, 2010, **184**, 855-863.
196. M. M. Khin, A. S. Nair, V. J. Babu, R. Murugana and S. Ramakrishna, *Energy Environ. Sci.*, 2012, **5**, 8075-8109.
197. H. L. Huang, W. M. G. Lee and F. S. Wu, *J. Hazard. Mater.*, 2016, **302**, 198-207.
198. S. Rodrigues, K. T. Ranjit, S. Uma, I. N. Martyanov and K. J. Klabunde, *Adv. Mater.*, 2005, **17**, 2467-2471.
199. J. Lyu, L. Z. Zhu and C. Burda, *Catal. Today*, 2014, **225**, 24-33.
200. P. Pichat, J. Disdier, C. Hoang-Van, D. Mas, G. Goutailler and C. Gaysse, *Catal. Today*, 2000, **63**, 363-369.
201. S. W. Verbruggen, S. R. Deng, M. Kurttepeli, D. J. Cott, P. M. Vereecken, S. Bals, J. A. Martens, C. Detavernier and S. Lenaerts, *Appl. Catal. B:Environ.*, 2014, **160-161**, 204-210.
202. N. Seifvand and E. Kowsari, *RSC Adv.*, 2015, **5**, 93706-93716.
203. W. K. Jo, J. Y. Lee and H. H. Chun, *Materials*, 2014, **7**, 1801-1813.
204. X. Y. Fan, F. M. Qiu, H. S. Yang, W. Tian, T. F. Hou, and X. B. Zhang, *Catal. Chem.*, 2011, **12**, 1298-1301.
205. N. H. Nguyen and H. Bai, *Appl. Surf. Sci.*, 2015, **355**, 672-680.
206. H. G. Yu, J. G. Yu and B. Cheng, *Chemosphere*, 2007, **66**, 2050-2057.
207. L. Ren, Y. Z. Li, J. T. Hou, J. L. Bai, M. Y. Mao, M. Zeng, X. J. Zhao and N. Li, *Appl. Catal. B:Environ.*, 2016, **181**, 625-634.

208. Z. R. Tang, F. Li, Y. H. Zhang, X. Z. Fu and Y. J. Xu, *J. Phys. Chem. C*, 2011, **115**, 7880-7886.
209. W. J. Ong, L. L. Tan, S. P. Chai and S. T. Yong, *Dalton Trans.*, 2015, **44**, 1249-1257.
210. W. J. Ong, L. K. Putri, L. L. Tan, S. P. Chai and S. T. Yong, *Appl. Catal. B:Environ.*, 2016, **180**, 530-543.
211. W. J. Ong, L. K. Putri, L. L. Tan, S. P. Chai, S. T. Yong and A. R. Mohamed, *Nano Energy*, 2015, **13**, 757-770.
212. L. B. Kuai, Y. Zhou, W. G. Tu, P. Li, H. J. Li, Q. F. Xu, L. Q. Tang, X. Y. Wang, M. Xiao and Z. G. Zou, *RSC Adv.*, 2015, **5**, 88409-88413.
213. T. Inoue, A. Fujishima, S. Konishi and K. Honda, *Nature*, 1979, **277**, 637-638.
214. L. L. Tan, W. J. Ong, S. P. Chai and A. R. Mohamed, *Chem. Commun.*, 2014, **50**, 6923-6926.
215. L. Yuan, C. Han, M. Pagliaro and Y. J. Xu, *J. Phys. Chem. C*, 2016, **120**, DOI: 10.1021/acs.jpcc.5b08893.
216. J. E. Benedetti, D. R. Bernardo, A. Morais, J. Bettinib and A. F. Nogueira, *RSC Adv.*, 2015, **5**, 33914-33922.
217. D. N. Chen, X. G. Zhang and A. F. Lee, *J. Mater. Chem. A*, 2015, **3**, 14487-14516.
218. M. Pelaez, N. T. Nolan, S. C. Pillai, M. K. Seery, P. Falaras, A. G. Kontos, P. S. M. Dunlop, J. W.J. Hamilton, J. A. Byrne, K. O'Sheaf, M. H. Entezari and D. D. Dionysiou, *Appl. Catal. B:Environ.*, 2012, **125**, 331-349.
219. K. Mori, H. Yamashita and M. Anpo, *RSC Adv.*, 2012, **2**, 3165-3172.
220. I. H. Tseng, W. C. Chang and J. C. S. Wu, *Appl. Catal. B:Environ.*, 2002, **37**, 37-48.
221. Y. Wang, Q. H. Lai, F. Zhang, X .D. Shen, M. H. Fan, Y. M. He and S. Q. Ren, *RSC Adv.*, 2014, **4**, 44442-44451.
222. L. L. Tan, W. J. Ong, S. P. Chai and A. R. Mohamed, *Appl. Catal. B:Environ.*, 2015, **166-167**, 251-259.
223. W. N. Wang, W. J. An, B. Ramalingam, S. Mukherjee, D. M. Niedzwiedzki, S. Gangopadhyay and P. Biswas, *J. Am. Chem. Soc.*, 2012, **134**, 11276-11281.
224. G. X. Ping, C. Wang, D. Chen, S. Liu, X. N. Huang, L. S. Qin, Y. X. Huang and K. Y. Shu, *J. Solid State Electrochem.*, 2013, **17**, 2503-2510.
225. X. J. Feng, J. D. Sloppy, T. J. LaTempa, M. Paulose, S. Komarneni, N. Z. Bao and C. A. Grimes, *J. Mater. Chem.*, 2011, **21**, 13429-13433.
226. O. K. Varghese, M. Paulose, T. J. LaTempa and C. A. Grimes, *Nano Lett.*, 2009, **9**, 731-737.
227. H. Xu, S. X. Ouyang, P. Li, T. Kako and J. H. Ye, *ACS Appl. Mater. Interfaces*, 2013, **5**, 1348-1354.
228. H. F. Dang, X. F. Dong, Y. C. Dong and J. S. Huang, *Int. J. Hydrogen Energy*, 2013, **38**, 9178-9185.
229. Z. C. Lian, W. C. Wang, S. N. Xiao, X. Li, Y. Y. Cui, D. Q. Zhang, G. S. Li and H. X. Li, *Sci. Rep.*, 2015, **5**, 10461.
230. M. Mollavali, C. Falamaki and S. Rohani, *Int. J. Hydrogen Energy*, 2015, **40**, 12239-12252.
231. J. Y. Huang, K. Q. Zhang and Y. K. Lai, *Int. J. Photoenergy*, 2013, **2013**, 761971.
232. Y. K. Li, H. M. Yu, W. Song, G. F. Li, B. L. Yi and Z. G. Shao, *Int. J. Hydrogen Energy*, 2011, **36**, 14374-14380.
233. M. Altomare, M. Pozzi, M. Allieta, L. G. Bettini and E. Selli, *Appl. Catal. B:Environ.*, 2013, **136**, 81-88.
234. D. P. Kumar, N. L. Reddy, M. M. Kumari, B. Srinivas, V. D. Kumari, B. Sreedhar, V. Roddatis, O. Bondarchuk, M. Karthik, B. Neppolian and M. V. Shankar, *Solar Energy Materials and Solar Cells*, 2015, **136**, 157-166.
235. X. Yang, L. Wu, L. P. Du and X. J. Li, *Catal. Lett.*, 2015, **145**, 1771-1777.
236. G. M. Wang, H. Y. Wang, Y. C. Ling, Y. C. Tang, X. Y. Yang, R. C. Fitzmorris, C. C. Wang, J. Z. Zhang and Y. Li, *Nano Lett.*, 2011, **11**, 3026-3033.
237. L. Zhang, N. Q. Pan and S. W. Lin, *Int. J. Hydrogen Energy*, 2014, **39**, 13474-13480.
238. Y. K. Lai, J. J. Gong and C. J. Lin, *Int. J. Hydrogen Energy*, 2012, **37**, 6438-6446.
239. L. Z. Long, J. Li, L. P. Wu and X. J. Li, *Mat. Sci. Semicon. Proc.*, 2014, **26**, 107-111.
240. Y. F. Yu, J. L. Ren and M. Meng, *Int. J. Hydrogen Energy*, 2013, **38**, 12266-12272.
241. H. Y. Wang, W. Zhu, B. C. Chong and K. Qin, *Int. J. Hydrogen Energy*, 2014, **39**, 90-99.
242. C. Han, Y. D. Wang, Y. P. Lei, B. Wang, N. Wu, Q. Shi and Q. Li, *Nano Research*, 2015, **8**, 1199-1209.
243. L. Chen, Y. Zhou, H. Dai, Z. D. Li, T. Yu, J. G. Liu and Z. G. Zou, *J. Mater. Chem. A*, 2013, **1**, 11790-11794.
244. B. K. Liu, Y. J. Sun, X. S. Wang, L. J. Zhang, D. J. Wang, Z. W. Fu, Y. H. Lin and T. F. Xie, *J. Mater. Chem. A*, 2015, **3**, 4445-4452.
245. H. Huang, L. Pan, C. K. Lim, H. Gong, J. Guo, M. S. Tse and O. K. Tan, *Small*, 2013, **9**, 3153-3160.
246. A. K. Chandiran, A. Yella, M. T. Mayer, P. Gao, M. K. Nazeeruddin and M. Gratzel, *Adv. Mater.*, 2014, **26**, 4309-4312.
247. M. D. Ye, X. R. Wen, M. Y. Wang, J. Iocozzia, N. Zhang, C. J. Lin and Z. Q. Lin, *Mater. Today*, 2015, **18**, 155-162.
248. Z. Seidalilir, R. Malekfar, H. P. Wu, J. W. Shiu and E. W. G. Diau, *ACS Appl. Mater. Interfaces*, 2015, **7**, 12731-12739.
249. L. Y. Chen, Z. S. Yang, C. Y. Chen, T. Y. Ho, P. W. Liu and H. T. Chang, *Nanoscale*, 2011, **3**, 4940-4942.
250. H. S. Kim, J. W. Lee, N. Yantara, P. P. Boix, S. A. Kulkarni, S. Mhaisalkar, M. Gratzel and N. G. Park, *Nano Lett.*, 2013, **13**, 2412-2417.
251. B. Oregan and M. Gratzel, *Nature*, 1991, **353**, 737-740.
252. S.-C. Yang, D.-J. Yang, J. Kim, J.-M. Hong, H.-G. Kim, I.-D. Kim and H. Lee, *Adv. Mater.*, 2008, **20**, 1059-1064.
253. X. Y. Tao, P. Ruan, X. Zhang, H. G. Sun and X. F. Zhou, *Nanoscale*, 2015, **7**, 3539-3547.
254. X. K. Xin, B. Li, J. Jung, Y. J. Yoon, R. Biswas and Z. Q. Lin, *Part. Part. Sysm. Charact.*, 2015, **32**, 80-90.
255. A. Hagfeldt, G. Boschloo, L. Sun, L. Kloo and H. Pettersson, *Chem. Rev.*, 2010, **110**, 6595-6663.
256. Z. Weng, H. Guo, X. Liu, S. Wu, K. W. K. Yeung and P. K. Chu, *RSC Adv.*, 2013, **3**, 24758-24775.
257. Y. Ohsaki, N. Masaki, T. Kitamura, Y. Wada, T. Okamoto, T. Sekino, K. Niihara and S. Yanagida, *Phys. Chem. Chem. Phys.*, 2005, **7**, 4157-4163.
258. K. Shankar, G. K. Mor, H. E. Prakasam, S. Yoriya, M. Paulose, O. K. Varghese and C. A. Grimes, *Nanotechnology*, 2007, **18**, 065707.
259. E. M. Jin, X. G. Zhao, J.-Y. Park and H.-B. Gu, *Nanoscale Res. Lett.*, 2012, **7**, 97.
260. R. A. Naphade, M. Tathavadekar, J. P. Jog, S. Agarkar and S. Ogale, *J. Mater. Chem. A*, 2014, **2**, 975-984.
261. H.-S. Kim and J. S. Suh, *RSC Adv.*, 2015, **5**, 74107-74114.
262. J. Zhang, Q. T. Li, S. Q. Li, Y. Wang, C. Ye, P. Ruterana and H. Wang, *J. Power Sources*, 2014, **268**, 941-949.
263. G. C. Li, M. Peng, W. X. Song, H. Wang and D. C. Zou, *Nano Energy*, 2015, **11**, 341-347.
264. M. Q. Lv, D. J. Zheng, M. D. Ye, J. Xiao, W. X. Guo, Y. K. Lai, L. Sun, C. J. Lin and J. Zuo, *Energy Environ. Sci.*, 2013, **6**, 1615-1622.
265. M.-H. Yeh, L.-Y. Lin, C.-Y. Chou, C.-P. Lee, H.-M. Chuang, R. Vittal and K.-C. Ho, *Nano Energy*, 2013, **2**, 609-621.
266. L. Yang and W. W.-F. Leung, *Adv. Mater.*, 2013, **25**, 1792-1795.
267. V. O. Williams, N. C. Jeong, C. Prasittichai, O. K. Farha, M. J. Pellin and J. T. Hupp, *Acs Nano*, 2012, **6**, 6185-6196.
268. N. Firoozi, H. Dehghani and M. Afrooz, *J. Power Sources*, 2015, **278**, 98-103.
269. Z. Du, H. Zhang, H. Bao and X. Zhong, *J. Mater. Chem. A*, 2014, **2**, 13033-13040.
270. Z. K. Zheng, W. Xie, Z. S. Lim, L. You and J. L. Wang, *Sci. Rep.*, 2014, **4**, 5721.
271. I. Mora-Sero and J. Bisquert, *J. Phys. Chem. Lett.*, 2010, **1**, 3046-3052.
272. M. X. Wu, X. Lin, Y. D. Wang and T. L. Ma, *J. Mater. Chem. A*, 2015, **3**, 19638-19656.
273. I. Concina and A. Vomiero, *Small*, 2015, **11**, 1744-1774.
274. V. I. Klimov and D. W. McBranch, *Phys. Rev. Lett.*, 1998, **80**, 4028-4031.
275. J. L. Duan, H. H. Zhang, Q. W. Tang, B. L. He and L. M. Yu, *J. Mater. Chem. A*, 2015, **3**, 17497-17510.
276. Z. Li, L. B. Yu, Y. B. Liu and S. Q. Sun, *Electrochim. Acta*, 2015, **153**, 200-209.
277. M. Akimoto, T. Toyoda, T. Okuno, S. Hayase and Q. Shen, *Thin Solid Films*, 2015, **590**, 90-97.
278. G. Zhu, L. K. Pan, T. Xu and Z. Sun, *ACS Appl. Mater. Interfaces*, 2011, **3**, 1472-1478.
279. H. L. Feng, W. Q. Wu, H. S. Rao, Q. Wan, L. B. Li, D. B. Kuang and C. Y. Su, *ACS Appl. Mater. Interfaces*, 2015, **7**, 5199-5205.
280. W. T. Sun, Y. Yu, H. Y. Pan, X. F. Gao, Q. Chen and L. M. Peng, *J. Am. Chem. Soc.*, 2008, **130**, 1124-1125.
281. C. Chen, M. D. Ye, M. Q. Lv, C. Gong, W. X. Guo and C. J. Lin, *Electrochim. Acta*, 2014, **121**, 175-182.

282. H. L. Feng, W. Q. Wu, H. S. Rao, L. B. Li, D. B. Kuang and C. Y. Su, *J. Mater. Chem. A*, 2015, **3**, 14826-14832.
283. H. L. Feng, W. Q. Wu, H. S. Rao, Q. Wan, L. B. Li, D. B. Kuang and C. Y. Su, *ACS Appl. Mater. Interfaces*, 2015, **7**, 5199-5205.
284. Z. Yang, C.-Y. Chen, P. Roy and H.-T. Chang, *Chem. Commun.*, 2011, **47**, 9561-9571.
285. G. C. Xing, N. Mathews, S. Y. Sun, S. S. Lim, Y. M. Lam, M. Gratzel, S. Mhaisalkar and T. C. Sum, *Science*, 2013, **342**, 344-347.
286. J. H. Park, J. Seo, S. Park, S. S. Shin, Y. C. Kim, N. J. Jeon, H. W. Shin, T. K. Ahn, J. H. Noh, S. C. Yoon, C. S. Hwang and S. I. Seok, *Adv. Mater.*, 2015, **27**, 4013-4019.
287. Z. M. Zhou, Z. W. Wang, Y. Y. Zhou, S. P. Pang, D. Wang, H. X. Xu, Z. H. Liu, N. P. Padture and G. L. Cui, *Angew. Chem. Int. Ed.*, 2015, **54**, 9705-9709.
288. L. Etgar, P. Gao, Z. S. Xue, Q. Peng, A. K. Chandiran, B. Liu, M. K. Nazeeruddin and M. Gratzel, *J. Am. Chem. Soc.*, 2012, **134**, 17396-17399.
289. M. He, D. J. Zheng, M. Y. Wang, C. J. Lin and Z. Q. Lin, *J. Mater. Chem. A*, 2014, **2**, 5994-6003.
290. H. Sun, J. Deng, L. B. Qiu, X. Fang and H. S. Peng, *Energy Environ. Sci.*, 2015, **8**, 1139-1159.
291. A. Kojima, K. Teshima, Y. Shirai and T. Miyasaka, *J. Am. Chem. Soc.*, 2009, **131**, 6050-6051.
292. J. Burschka, N. Pellet, S.-J. Moon, R. Humphry-Baker, P. Gao, M. K. Nazeeruddin and M. Graetzel, *Nature*, 2013, **499**, 316-319.
293. Y. Liu, S. L. Ji, S. X. Li, W. W. He, K. Wang, H. B. Hu and C. H. Ye, *J. Mater. Chem. A*, 2015, **3**, 14902-14909.
294. N. Marinova, W. Tress, R. Humphry-Baker, M. I. Dar, V. Bojinov, S. M. Zakeeruddin, M. K. Nazeeruddin and M. Gratzel, *ACS Nano*, 2015, **9**, 4200-4209.
295. G. C. Xing, B. Wu, S. Chen, J. Chua, N. Yantara, S. Mhaisalkar, N. Mathews and T. C. Sum, *Small*, 2015, **11**, 3606-3613.
296. X. Y. Wang, Z. Li, W. J. Xu, S. A. Kulkarni, S. K. Batabyal, S. Zhang, A. Y. Cao and L. H. Wong, *Nano Energy*, 2015, **11**, 728-735.
297. Q. L. Jiang, X. Sheng, Y. X. Li, X. J. Feng and T. Xu, *Chem. Commun.*, 2014, **50**, 14720-14723.
298. S.-S. Li, Y.-C. Wang, C.-M. Tsai, C.-Y. Wen, C.-H. Yu, Y.-P. Yang, J.-C. Lin, D.-Y. Wang, C.-C. Chen, Y.-C. Yeh and C.-W. Chen, *Nanoscale*, 2015, **7**, 14532-14537.
299. A. Fakharuddin, F. Di Giacomo, A. L. Palma, F. Matteocci, I. Ahmed, S. Razza, A. D'Epifanio, S. Licoccia, J. Ismail, A. Di Carlo, T. M. Brown and R. Jose, *ACS Nano*, 2015, **9**, 8420-8429.
300. S. Hu, W. Chen, J. Zhou, F. Yin, E. Uchaker, Q. F. Zhang and G. Z. Cao, *J. Mater. Chem. A*, 2014, **2**, 7862-7872.
301. L. Y. Zhang, Y. Y. Wang, B. Peng, W. T. Yu, H. Y. Wang, T. Wang, B. W. Deng, L. Y. Chai, K. Zhang and J. X. Wang, *Green Chem.*, 2014, **16**, 3926-3934.
302. K. X. Wang, X. H. Li and J. S. Chen, *Adv. Mater.*, 2015, **27**, 527-545.
303. Y. X. Tang, Y. Y. Zhang, X. H. Rui, D. P. Qi, Y. F. Luo, W. R. Leow, S. Chen, J. Guo, J. Q. Wei, W. L. Li, J. Y. Deng, Y. K. Lai, B. Ma, X. D. Chen, *Adv. Mater.*, 2016, **28**, DOI: 10.1002/adma.201505161.
304. H. Lee, M. Yanilmaz, O. Toprakci, K. Fu and X. W. Zhang, *Energy Environ. Sci*, 2014, **7**, 3857-3886.
305. Y. X. Tang, Y. Y. Zhang, W. L. Li, B. Ma and X. D. Chen, *Chem. Soc. Rev.*, 2015, **44**, 5926-5940.
306. L. Peng, H. J. Zhang, Y. J. Bai, Y. Zhang and Y. Wang, *Nanoscale*, 2015, **7**, 8758-8765.
307. J. Qu, J. E. Cloud, Y. A. Yang, J. N. Ding and N. Y. Yuan, *ACS Appl. Mater. Interfaces*, 2014, **6**, 22199-22208.
308. D. D. Yuan, W. L. Yang, J. F. Ni and L. J. Gao, *Electrochim. Acta*, 2015, **163**, 57-63.
309. H. R. Xia, J. Li, C. Peng, W. T. Sun, L. W. Li and L. M. Peng, *ACS Appl. Mater. Interfaces*, 2014, **6**, 17376-17383.
310. H. Zheng, S. Fang, Z. K. Tong, G. Pang, L. F. Shen, H. S. Li, L. Yang and X. G. Zhang, *J. Mater. Chem. A*, 2015, **3**, 12476-12481.
311. A. R. Armstrong, G. Armstrong, J. Canales, R. Garcia and P. G. Bruce, *Adv. Mater.*, 2005, **17**, 862-865.
312. G. Armstrong, A. R. Armstrong, P. G. Bruce, P. Reale and B. Scrosati, *Adv. Mater.*, 2006, **18**, 2597-2600.
313. J. Y. Liao and A. Manthiram, *Adv. Energy Mater.*, 2014, **4**, 1400403.
314. W. Wang, M. Tian, A. Abdulagatov, S. M. George, Y. C. Lee and R. G. Yang, *Nano Lett.*, 2012, **12**, 655-660.
315. B. L. Wang, Q. Chen, J. Hu, H. Li, Y. F. Hu and L. M. Peng, *Chem. Phys. Lett.*, 2005, **406**, 95-100.
316. J. M. Li, W. Wan, H. H. Zhou, J. J. Li and D. S. Xu, *Chem. Commun.*, 2011, **47**, 3439-3441.
317. Y. Q. Zhang, Q. Fu, Q. L. Xu, X. Yan, R. Y. Zhang, Z. D. Guo, F. Du, Y. J. Wei, D. Zhang and G. Chen, *Nanoscale*, 2015, **7**, 12215-12224.
318. J. R. Li, Z. L. Tang and Z. T. Zhang, *Chem. Mater.*, 2005, **17**, 5848-5855.
319. X. Xu, Z. Y. Fan, S. J. Ding, D. M. Yu and Y. P. Du, *Nanoscale*, 2014, **6**, 5245-5250.
320. M. L. Mao, L. Mei, D. Guo, L. C. Wu, D. Zhang, Q. H. Li and T. H. Wang, *Nanoscale*, 2014, **6**, 12350-12353.
321. B. Chen, N. Q. Zhao, L. C. Guo, F. He, C. S. Shi, C. N. He, J. J. Li and E. Z. Liu, *Nanoscale*, 2015, **7**, 12895-12905.
322. C. Wang, L. X. Wu, H. Wang, W. H. Zuo, Y. Y. Li and J. P. Liu, *Adv. Funct. Mater.*, 2015, **25**, 3524-3533.
323. J. Y. Liao, D. Higgins, G. Lui, V. Chabot, X. C. Xiao and Z. W. Chen, *Nano Lett.*, 2013, **13**, 5467-5473.
324. Z. X. Yang, G. D. Du, Q. Meng, Z. P. Guo, X. B. Yu, Z. X. Chen, T. L. Guo and R. Zeng, *J. Mater. Chem.*, 2012, **22**, 5848-5854.
325. B. T. Zhao, R. Cai, S. M. Jiang, Y. J. Sha and Z. P. Shao, *Electrochim. Acta*, 2012, **85**, 636-643.
326. X. Zhang, Y. K. Lai, M. Z. Ge, Y. Zheng, K. Q. Zhang and Z. Q. Lin, *J Mater. Chem. A*, 2015, **3**, 12761-12768.
327. Y. P. Fu, X. Cai, H. W. Wu, Z. B. Lv, S. C. Hou, M. Peng, X. Yu and D. C. Zou, *Adv. Mater.*, 2012, **24**, 5713-5718.
328. V. T. Le, H. Kim, A. Ghosh, J. Kim, J. Chang, Q. A. Vu., D. T. Pham, J.-H. Lee, S.-W. Kim and Y. H. Lee, *ACS Nano*, 2013, **7**, 5940-5947.
329. T. Chen, R. Hao, H. S. Peng and L. M. Dai, *Angew. Chem. Int Ed.*, 2015, **54**, 618-622.
330. S. W. Pan, J. Deng, G. Z. Guan, Y. Zhang, P. N. Chen, J. Ren and H. S. Peng, *J. Mater. Chem. A*, 2015, **3**, 6286-6290.
331. M. Salari, S. H. Aboutalebi, K. Konstantinov and H. K. Liu, *Phys. Chem. Chem. Phys.*, 2011, **13**, 5038-5041.
332. A. Ramadoss and S. J. Kim, *J Alloy. Compd.*, 2013, **561**, 262-267.
333. Y. G. Wang, Z. D. Wang and Y. Y. Xia, *Electrochim. Acta*, 2005, **50**, 5641-5646.
334. D. D. Zhu, Y. D. Wang, G. L. Yuan and H. Xia, *Chem. Commun.*, 2014, **50**, 2876-2878.
335. J.-H. Kim, K. Zhu, Y. Yan, C. L. Perkins and A. J. Frank, *Nano Lett.*, 2010, **10**, 4099-4104.
336. Q. Q. Tan, Y. X. Xu, J. Yang, L. L. Qiu, Y. Chen and X. X. Chen, *Electrochim. Acta*, 2013, **88**, 526-529.
337. S. F. Jiang, B. L. Yi, C. K. Zhang, S. Liu, H. M. Yu and Z. G. Shao, *J. Power Sources*, 2015, **276**, 80-88.
338. L. M. Li, X. M. Zhang, G. S. Wu, X. Peng, K. F. Huo and P. K. Chu, *Adv. Mater. Interfaces*, 2015, **2**, 1400446.
339. Z. Shao, H. J. Li, M. J. Li, C. P. Li, C. Q. Qu and B. H. Yang, *Energy*, 2015, **87**, 578-585.
340. X. L. Chen, H. Sun, Z. B. Yang, G. Z. Guan, Z. T. Zhang, L. B. Qiu and H. S. Peng, *J Mater. Chem. A*, 2014, **2**, 1897-1902.
341. A. Ramadoss, G.-S. Kim and S. J. Kim, *CrystEngComm*, 2013, **15**, 10222-10229.

The state-of-the-art development of fabrication method and surface engineering strategies of 1D TiO_2 nanostructures is reviewed first. And then is followed by an overview of their potential applications in various applications including photocatalysts for pollutant degradation/CO_2 photoreduction, water splitting, solar cells, lithium-ion batteries and supercapacitors.

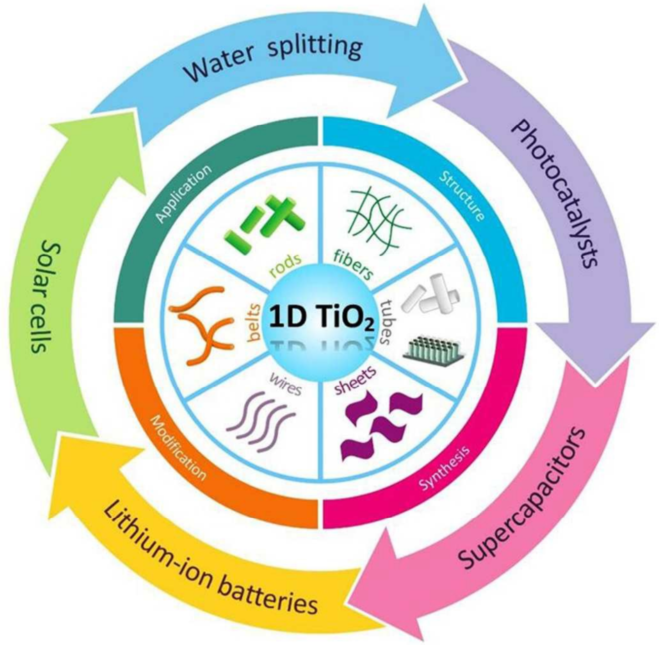

Mingzheng Ge received his M.S. degree in College of Textile and Clothing Engineering at Soochow University in 2015. He is currently pursuing a Ph.D. degree under Prof. Yuekun Lai and Prof. Keqin Zhang in College of Textile and Clothing Engineering at Soochow University. His research interests include inorganic semiconductor advanced materials and their application in photocatalytic degradation, water splitting, supercapacitors, dye-sensitized solar cells and lithium-ion batteries.

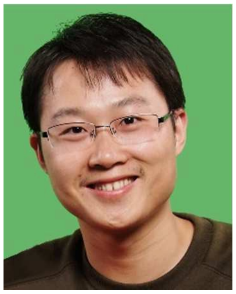

Yuekun Lai is a full professor at National Engineering Laboratory for Modern Silk, and School of Textile and Clothing Engineering in Soochow University since 2013. He received his Ph.D. degree from the Department of Chemistry, Xiamen University. During 2009-2011, he worked as a research fellow at Nanyang Technological University, Singapore. At July of 2011, he moved to Muenster University with Prof. Harald Fuchs and Prof. Lifeng Chi under the support of Humboldt Scholarship of Germany. His research interests are focused on TiO_2 nanostructures for energy & environmental applications, bio-inspired intelligent surfaces with special wettability.